ANALYZING THE EFFECTS OF LAND COVER/LAND USE CHANGES ON FLASHFLOOD: A CASE STUDY OF MARIKINA RIVER BASIN (MRB), PHILIPPINES

BREBANTE, BEVERLY MAE
March, 2017

SUPERVISORS:
Dr. D. B. P. Shrestha
Dr. D. Alkema

ANALYZING THE EFFECTS OF LAND COVER/LAND USE CHANGES ON FLASHFLOOD: A CASE STUDY OF MARIKINA RIVER BASIN (MRB), PHILIPPINES

BREBANTE, BEVERLY MAE
Enschede, The Netherlands, March, 2017

Thesis submitted to the Faculty of Geo-Information Science and Earth Observation of the University of Twente in partial fulfilment of the requirements for the degree of Master of Science in Geo-information Science and Earth Observation.
Specialization: Applied Earth Sciences – Natural Hazards, Risk and Engineering

SUPERVISORS:
Dr. D. B. P. Shrestha
Dr. D. Alkema

THESIS ASSESSMENT BOARD:
Prof. Dr. V.C., Jetten (Chair)
Dr. T.A, Bogaard (External Examiner, Delft University of Technology)

ABSTRACT

Flooding is one of the most common type of hydrological hazards that affects various countries in varying degrees. World-wide, flooding results to population displacement, damage to properties, disruption of economic activities and loss of life. Flooding is of particular concern for the Philippines and for many developing countries vulnerable to high levels of rainfall. Flooding is generally caused by intense precipitation over a short duration or by normal rain over a longer period of time, but study shows that some anthropogenic activities such as land use or land cover changes, channel modification, deforestation and urbanization also influence the occurrence of this hazard. In this research, the influence of LULC change to runoff generation and flashflood was evaluated particularly in the Marikina River Basin (MRB).

LULC classification was initially established from 1989 Landsat TM imagery and 2016 Landsat OLI imagery of the study area and was then subjected to change detection. The classified images were then used to simulate flood scenarios using a physically-based hydrological model. The extreme rainfall of Typhoon Ketsana and generated rainfall of various return periods (5y-, 10y, and 20y-RP) were used as input data for the simulation.

Results show that the influence of LULC change varies on the upper catchment and lower floodplains of MRB. Analysis of the upstream area showed that the change of vegetative cover have an insignificant effect to runoff generation during convective or extreme conditions. In the downstream part, urbanization have an effect on flood extent, flood volume and flood duration. Moreover, simulation of scenarios using design storm of 5y-, 10-y and 20-y return period revealed that increase of rainfall intensity diminishes the influence of vegetative land covers to flood characteristics.

ACKNOWLEDGEMENTS

My utmost gratefulness to the Lord God Almighty, from whom all things are made possible. It is by His grace that brought me here to start a new chapter of my life. To God be the Glory.

I thank the Netherlands Fellowship Programmes (NFP) for extending their support in my studies which paved the way to pursue my Master's Degree and to the Mines and Geosciences Bureau for granting me this opportunity and supporting me all the way in finishing my research work.

I am deeply grateful to my supervisors, Dr. Dhruba and Dr. Alkema, for providing me the guidance, critics and encouragement from the beginning of my research proposal until the completion of my thesis. To Dr. Jetten, for untiringly sharing his expertise in openLISEM. To Dr. Lievens, for her patience in teaching and training in laboratory works. To Dr. Parodi, for spending part of his time remotely in clearly explaining how HECRAS works. To Bart Krol for being our constant support this whole MSc program.

Also, I would like to express my deepest gratitude to all the instructors and staff of ITC for imparting valuable lessons from their extensive experiences. To my AES family especially, who have been with me in this journey and kept me motivated in every step of the way.

Special thanks to the ITC Filipino community, you've made my short stay here full of laughter and cook-out dinner. My ICF family for always being my home away from home. Thank you for the moral sustenance, for sharing your own light when I felt darkness and despair was all that is left. Thank you for your consistent prayers and reminders that all will be well through Christ.

I also express my eternal gratitude to my family (Mom, Dad, John, Mich, DJ, Chris, Zy and Memec) for always being my foundation and ceaseless source of strength. Your unconditional love and endless support and prayers gave me the reason to face all my challenges with a smile.

Lastly, I dedicate this fruit of my labor, to my son Gab, for being my inspiration. Your love and understanding have sustained all the hardships and longing all worth it.

TABLE OF CONTENTS

LIST OF FIGURES

LIST OF TABLES

1. INTRODUCTION

1.1. Background

Over the past decades, different weather-related disasters have been affecting various countries resulting to loss of numerous lives, damaged properties and significantly disrupted economic activities. Among all weather-related disasters (1995-2015), 47% is attributed to flooding which have affected 2.3 billion people, the majority of whom (95%) live in Asia (Wahlstrom & Guha-Sapir, 2015; EM-DAT, 2016). In the 21st century, notable examples of flood events in a global scale include the 2000 Mozambique flood in Southern Africa, which was caused by successive extreme rainfall events for several months resulting to swelling of some rivers twice the normal water level ("List of Floods", 2017). The 2004 Haiti flood resulted in 600 casualties after two days of continuous rain. In 2006, tens of thousands of people across south-eastern Europe suffered from flood waters due to the swelling of the Danube River ("BBC News," 2014).

In Asia, flooding is a normal occurrence affecting thousands of people especially in developing countries like India, Bangladesh, China, Vietnam, Pakistan and Indonesia. This is mainly attributed to the large and heterogeneous land masses consisting of multiple river basins and flood plains coupled with high-population densities along flood-prone areas (Wahlstrom & Guha-Sapir, 2015). In the report on the Southeast Asia Flood Situation by the Food and Agriculture Organization of the United Nations (2016), severe localized flooding events during the first half of the 2016 monsoon season were mentioned. This included the localized flooding in Bangladesh brought about by heavy monsoon rains in mid-July affecting at least 3.7 million people and damaging thousands of houses (Food and Agriculture Organization of the United Nations, 2016). The localized flood in Nepal affected 36 of the country's 75 districts, while the flooding in India impacted the north-eastern parts of the country due to above-average monsoon rainfall. Other localized flood mentioned in the report occurred in China, Myanmar and Sri Lanka. In 2011, Thailand experienced its worst flooding brought by above-average rainfall, enhanced by extreme precipitation from four tropical storm remnants affecting 65 out of 77 provinces (Gale & Saunders, 2013).

The Philippines, one of the tropical country in Southeast Asia, is considered by the United Nations Office for Disaster Risk Reduction (UNISDR) as one of the top five most disaster-prone countries worldwide. In the last decade, the Philippines was devastated by several major flood events, including the 2009 flooding of Metro Manila caused by Typhoon Ketsana that generated 6-meter high flood waters in rural areas. Currently, flood frequency accounts to about 32% of the natural hazards affecting the country ("Global Assessment Report on Disaster Risk Reduction 2015," n.d.).

Flooding is one of the most common type of hydrological hazards due to the vast geographical distribution of river floodplains and low-lying coastal areas ("Natural Disaster Association," n.d.). It is generally caused by intense precipitation over a short duration or by normal rain over a longer period of time. But study shows that some anthropogenic activities such as land use or land cover (LULC) changes, channel modification, deforestation and urbanization also influence the occurrence of this hazard (Ramesh, 2013) and a number of studies mostly focus on the effects of LULC change.

LULC patterns may be attributed to the geologic and geomorphologic setting of an area, or can be associated to the socioeconomic factors and its utilization in time and space (Zubair, 2006). However, geologic processes such as erosion and weathering, varying weather patterns and climate change as well as changing demands in the economy influence the inevitable changes of LULC. Studies show that these changes either influenced by natural or anthropogenic activities have a significant impact in watershed processes particularly in the hydrological system (Aich et al., 2016; Rawat et al., 2013; Zope et al., 2016).

Previous works have been undertaken in the last decades which aimed at recognizing and evaluating the influence of land use to flooding. A case study in Maying River catchment in China concluded that the conversion of woodland and grassland to cultivated lands in the upstream portion resulted to the decrease in mean annual run-off, base flow, maximum peak discharge and mean discharge in spring and autumn (Wang, Zhang, Liu, & Chen, 2006a). In contrast, another study showed that land use change from forest and rangelands into cultivated areas resulted to an increase of flood peak and volume (Saghafian, Farazjoo, Bozorgy, & Yazdandoost, 2008). Ramesh (2013) stated that urbanization within the floodplain area, as well as installation of structural flood measures, also reduce the capacity for storage and infiltration as well as limit flow pathways for surface run-off that can lead to inundation.

The extensive research regarding hydrological processes particularly flooding, is attributed to the increasing availability of free and commercial remote sensed data and the development of several sophisticated techniques, which provide new tools for advanced analysis of processes in a watershed system (Prawiranegara, 2014). In image classification, detailed land use and land cover maps were generated using Landsat-5/TM, MODIS, and PRODES (INPE 2015) while SPOT 5 was used for validation (Almeida et al. , 2016). Very high resolution images such as IKONOS and QUICKBIRD were utilized in the work of Deng et al. (2009) in analysing spatio-temporal characteristics of land use change for understanding and assessing ecological consequence of urbanization.

Most studies on flooding use hydrological modelling such as rainfall-runoff models which initially started in simple models and has now advanced into complex algorithms that can take into account the variability of watershed conditions (Džubáková, 2010). Some examples of models include Saghafian et al. (2008) work that used Hydrologic Engineering Center's Hydrologic Modelling System (HEC-HMS) Model to simulate hydrologic response while in the work of Ramesh (2013), he used hydrodynamic models namely HEC-GeoRAS Model and SOBEK Model to estimate flood propagation. The hydrological model SWAT (soil and water assessment tool) and Limburg Soil Erosion Model (LISEM) were also introduced in other research studies (Zhang et al., 2016; Kværnø & Stolte, 2012).

The objective of hydrologic modelling is to understand the hydrologic processes or phenomena within a watershed and of how changes within the watershed may affect this phenomena. It also aims to generate synthetic sequences of hydrologic data for facility design or for use in forecasting and provide valuable information for studying the potential impacts of changes in land use or climate (Xu, 2002).

This research aims to characterize the response of a large watershed particularly the Marikina River Basin to significant LULC change. MRB is the largest river basin draining to Metropolitan Manila (Abon et al., 2016) and serves as the headwater that causes flood downstream (Badilla, 2008). In this study, flood simulation will be generated using physically -based hydrological model taking into account a single extreme rainfall event and various return periods.

1.2. Problem Description

In the Philippines, land use conversion is rapidly occurring in response to land development or urbanization, industrialization and increasing demand for certain agricultural produce. Forest areas are being encroached and converted to plantations or agricultural lands that cause vegetation degradation thus minimizing interception capacity. Urbanization, on the other hand, involves construction of hard surfaces such as houses, paved roads, infrastructure development, and congestion of drainage systems which reduced infiltration and increase overland flow. These, in effect, may result to the aggravation of flooding occurrences in the future (Suriya & Mudgal, 2012).

Although numerous studies have been undertaken in Marikina River Basin in studying the influence of LULC change in flooding, more research are needed given the emergence of new data sources, and development of new hydrological models. How to generate and improve flood simulation and forecasting, through incorporating additional parameters considered significant in flood analysis of a large catchment is the main research problem of this research.

The output of this research will provide a better understanding on the influence of various LULC to floods by analysing the correlation with the past and existing land uses to the occurrence of flooding.

1.3. Research Objectives

This research aims to determine the impact of LULC change in Marikina River Basin on flooding. This study mainly focuses on land cover/land use change, to contribute and provide significant information to local planners in the enhancement of comprehensive land use plans within the study area.

1.3.1. Specific Objectives and Research Question

To achieve the main objective, the following specific objectives are as follows:

- To detect significant land cover/land use change in MRB within the last decades.
    - What are the main driving forces that may have contributed to the land use change within the study area?

- To evaluate the influence of various LULC change to overland flow with extreme rains of different return periods.
    - What is the impact of the different LULC type to the generation of surface runoff and flood characteristics?
    - What LULC type is runoff generation most sensitive in terms of volume and timing?

1.4. Thesis Structure

This thesis report is composed of seven chapters, as listed and described below:

Chapter 1	Introduction	This chapter contains the general overview of the research work, which includes the research problem and its related objectives and questions. The extent of the study and limitations that were considered in the work were also stated in this chapter.
Chapter 2	Literature Review	Information on concepts, methodology and other related data gathered from previous studies and literature are discussed in this Chapter.
Chapter 3	Study Area	Description of the location, geomorphology, climate, land cover and underlying soil units of the study are is mentioned in this chapter.
Chapter 4	Methodology	In this chapter, the research approach will be discussed and the required dataset for the flood simulation as well as the source of information and description is presented. Procedures of the laboratory analysis, image analysis and flood modelling will also be stated in detail.
Chapter 5	Results and Discussion	Contains the outputs of laboratory works, image analysis and flood simulations illustrated using maps, graphs and tables. Results will be thoroughly discussed in this chapter to fulfil the above-mentioned objectives and answer research questions.
Chapter 6	Conclusion and Recommendation	Describes the conclusion obtained from the analysis of results and presents the recommendation that should be taken into consideration for future research works.

2. LITERATURE REVIEW

2.1. Flooding and its influencing factors

Flooding is generally associated with weather conditions which generate excessive volume of surface runoff that exceeds the storage capacity of natural and artificial drainages. In an extreme event such as high rain intensity in a short duration, infiltration capacity of the underlying soil as well as interception capacity of vegetation may be exceeded. This results in the accumulation of water on the surface which will eventually flow downslope as overland flow mainly due to gravity (Dimitriou, 2011; Liu et al., 2004). Overland flow (or surface runoff) is defined as the movement of water over the Earth's surface towards low lying areas, ending up in a body of water (Dimitriou, 2011).

Overland flow can either be generated through infiltration excess also known as Hortonian overland flow (HOF) or soil saturation excess known as saturation overland flow (SOF). Generally, convective rainstorms with high intensity and usually short duration are more likely to produce Hortonian overland flow (HOF) while long-duration advective events with low intensity typically produce saturation overland flow (SOF) (Kirkby, 1988; Steinbrich et al., 2016).

One key factor influencing overland flow is land use and land cover particularly in the infiltration process due to its interception capacity, deposition of surface mulch and ability to alter pore-size distribution of soil through aggregation and root penetration (Dunne, 1983). Grassland pasture for instance as compared to forest cover, has a higher surface albedo, lower surface roughness, lower leaf area and shallower rooting depth leading to reduced evapotranspiration (ET) and increase in long-term discharge. In addition, with lower leaf area and less litter, rainfall interception is less and surface capacity detention is decreased, thus a substantial amount of rainfall runs off as overland flow (Costa et al., 2003). Archer et al.(2013) added that broadleaf woodlands planted on hillslopes in clusters or shelterbelts within grassland can provide areas of high infiltration capacity and subsequently prevent run-off generation during flood-producing storm events. In the work of Sriwongsitanon & Taesombat (2011), they concluded that forest cover has a varying effect on runoff coefficient depending on the severity of storm events, different stages of antecedent soil moisture and other factors.

Besides LULC and rainfall, dynamics of overland flow formation is also controlled by topographic factors of terrain slope and elevation and pedological physical properties (permeability, texture and antecedent soil moisture) (Dimitriou, 2011; Penna et al., 2011; Petrović, 2016). In a watershed, two landscape units namely the hillslope zones and the riparian zones are generally considered as a controlling factor in runoff generation (McGlynn & McDonnell, 2003). According to the paper, hillslope and riparian zones exhibit distinct hydrological characteristics due to their location in the catchment and distinctive slope characteristics such as local slope angle and upslope contributing area. In recent research works (McGlynn et al., 2004; Penna et al., 2011), it was concluded that during small rainfall events, runoff is typically generated in riparian zones however during wetter antecedent conditions or larger precipitation events, hillslopes become a major contributor to storm runoff.

Topographic properties of hillslopes are important in the generation of storm runoff (Fujimoto et al., 2011). During small rainfall events in small catchments, runoff is predominantly attributed to runoff from the side slopes (divergent and/or planar type of hillslope) and as precipitation increases, the valley-head (convergent type of hillslope) starts to additionally contribute to the catchment runoff (Fujimoto et al., 2011). Dunne (1983) added that convergent topography generated particularly high runoff rates. Moreover, in large catchments, water flow pathways during and between rainfall events largely depends on slope morphology (Beven et al., 1988).

Moreover, soil physical properties affect the infiltration capacity within a watershed. Infiltration capacity of soils is defined as the maximum rate at which a given soil can absorb surface water input in a given situation (Horton, 1940). This varies within a catchment area due to spatial variability of soil such as initial moisture content, hydraulic conductivity of the soil profile, texture, structure, porosity, bulk density and organic matter content (Tarboton, 2003; Horton, 1945; Hillel, 1998; Bi et al., 2014).

Infiltrability is directly proportional to hydraulic conductivity (Hillel, 1998) and a change of which plays a decisive role in generating flow paths for overland flow (Elsenbeer, 2001). The hydraulic conductivity of the soil is greatly influenced by particle size distribution (percentage of sand, silt and clay), organic matter content (OM) and structure (Haghnazari et al., 2015). Antecedent soil moisture also plays a role in infiltration of rain water, especially in a pore system of a heterogeneous soil section wherein the hydraulic potential along wider pore spaces depends on how much of the spaces have been previously filled up with moisture (Kirkby, 1988). In dry conditions during small storms, less amount of stormflow is generated mainly from the overland flow from the riparian zone which is characterized by high soil moisture conditions and is therefore prone to rapid runoff response. However, in wet conditions and larger rain events when soil moisture threshold is exceeded, there will be higher runoff ratios predominantly contributed by runoff from hillslopes (Penna et al., 2011).

Soil bulk density on the other hand is a measure of soil compaction (Dudley et. al., 2002) and is inversely related to soil infiltration, which is an important indicator of soil infiltration ability. When bulk density is lower, soil infiltration depth is greater which indicates that more water can precipitate into the soil thus reducing surface runoff (Bi et al., 2014).

As mentioned earlier, these soil properties are related to the existing land use and land cover within the watershed. Therefore, changes in LULC can directly affect soil integrity, nutrient fluxes and native species assemblages which in turn may alter certain soil properties like porosity, bulk density, saturated hydraulic conductivity (Kfs) or surface soil permeability (Chappell et al., 1996) and surface roughness (Saghafian et al., 2008). Significant variation in these soil properties and variables can influence the rates of interception, infiltration, evapotranspiration and groundwater recharge (Archer et al., 2013; Baker & Miller, 2013) that may result to changes in a watershed hydrologic response (Baker & Miller, 2013; Wang et al., 2006a). In some case studies in China and Iran, alteration of land uses such as from woodland to cultivated lands resulted to a change in mean annual run-off, base flow, maximum peak discharge and mean discharge (Saghafian et al., 2008; Wang et al., 2006)

In most hydrological studies, land use and land cover change are given more emphasis because of its direct relevance to many environmental and socioeconomic applications such as flood management and formulation of comprehensive land use plans (Almeida et al., 2016; Lu & Weng, 2007).

2.2. Land use and land cover change (LULCC) impact on flood and change detection analysis

Studies show that changes in land use/land cover either influenced by natural or anthropogenic activities have a significant impact on watershed processes particularly in the hydrological system (Aich et al., 2016; Rawat et al., 2013; Zope et al., 2016). The changes alter the balance between rainfall and evaporation and, consequently, the runoff response in the area (Costa et al., 2003). In the same work, the author added that in a large watershed particularly, long-term discharge is altered primarily by precipitation variability and changes in LULC in the upstream basin. Ramesh (2013) also added that urbanization within the floodplain area as well as installation of structural flood measures also reduce the capacity for storage and infiltration as well as limit flow pathways for surface run-off that can lead to inundation.

In analysing LULC change, remote sensing image classification is generally the initial step in this type of research work. Since the emergence of space-borne and airborne-based data coupled with various technological advances in remote sensing techniques and Geographical Information System (GIS), LULC classification has been the subject of many studies (Manakos & Braun, 2014; Prawiranegara, 2014). Procedure for image classification involves several steps e.g. selection of appropriate images, pre-processing, selection of training samples, selection of suitable classification algorithm, post classification processing and accuracy assessment (Lu & Weng, 2007). Moreover, these considerations depend largely on the user's requirement for the research work.

In general, classification techniques can be categorized into unsupervised and supervised, or parametric and non-parametric, or hard and soft (fuzzy) classification, or per-pixel, sub-pixel and per-field (Lu & Weng, 2007). However, if utilized improperly, the classification algorithms may cause unnecessary errors of omission and commission (Smits et al.,1999). Traditional classifiers such as K-nearest neighbour (KNN) or maximum likelihood (ML) may operate well on Landsat TM datasets but are not fitting for e.g. backscatter radar signals of SAR (Smits et al., 1999). Based on the comparison of some classification algorithm in one research paper (Li et al., 2014), results show that for pixel-based classification, logistic regression (LR) gave the best accuracy for the 6-band while maximum likelihood classifier produced the highest accuracy for the 4-band case. In addition, for object-oriented method where classification is largely dependent on segmentation, stochastic gradient boosting (SGB) has the best performance. Lu & Weng (2007), proposed that the use of ancillary data such as topography, soil, road and census data, may be utilized with remotely sensed data to improve classification performance.

Once LULC maps are generated, change detection analysis can be undertaken. Change detection is the process of identifying differences in the state of an object or phenomenon by observing it at different times (Singh, 1989). In relation to land cover, Lillesand & Kiefer (1987) stated that change detection involves the use of multi-temporal datasets to discriminate areas of change between dates of imaging. Major and most sources of satellite imageries for change detection include Landsat's Thematic Mapper (TM), Enhanced TM Plus (ETM+) and Operational Land Imager (OLI), Satellite Probatoire d' Observation de la Terre (SPOT), Radar and Advanced Very High Resolution Radiometer (AVHRR), Moderate Resolution Imaging Spectroradiometer (MODIS) and Advanced Spaceborne Thermal Emission and Reflection Radiometer (ASTER) (Lu et al., 2004; Wu et al., 2016) due to their public availability, long record of image acquisition, wide spatial coverage and near nadir observations (ESA Earth online, n.d.).

Various LULC change detection techniques have now been developed which takes into account the spatial, spectral, thematic and temporal constraints (Hu & Zhang, 2013). These methods can be grouped in three broad main categories based on the data transformation procedures and the analysis techniques used to delimit areas of significant changes: (1) image enhancement, (2) multi-date classification and (3) comparison of two independent land cover classification (Mas, 1999a).

Image enhancement approach involves algebra or mathematical combination of imagery from different dates to increase the visual distinction between features (Lillesand, 1987). This includes subtraction of bands, rationing, image regression or principal component analysis (PCA), change vector analysis, vegetation index differencing, etc (Mas, 1999; Lillesand, 1987). The direct multi-date classification is based on the single analysis of a combined dataset of two or more different dates, in order to identify areas of changes statistically (Mas, 1999b). Post-classification comparison involves independently produced spectral classification results from each time of interest, followed by a pixel-by –pixel or segment-by-segment comparison to detect changes (Coppin et al., 2004; Ilsever & Unsalan, 2012). It is a common and popular approach for change detection as it provides “from-to” change information and minimizes the impact of sensor and environmental differences, but has some limitation in classifying historical image data (Lu et al., 2004).

To better understand the impacts of land cover changes to occurrences of flooding, understanding of hydrological processes within a watershed system become important. Hydrologic modelling is used by researchers to simulate hydrologic processes in the catchment.

2.3. Hydrologic Model

Development and application of rainfall-runoff modelling started in the 19th century (Xu, 2002) and evolved into a complex algorithms with the advances and emergence of new technologies that incorporate inter-related variables which have major influence to hydrological processes.

Džubáková (2010) categorized rainfall-runoff models into (1) metric (also called data-based, empirical or black box), (2) parametric (also called conceptual, explicit soil moisture accounting or grey box), and (3) mechanistic (also called physically based or white box) model structures.

Metric models are observation oriented models which take only information from existing data without considering the features and processes of hydrological systems (Devi et al., 2015). This model treats the catchment as a single unit and is site specific for the catchment’s condition, thus cannot be generalized and replicated to other watershed conditions (Džubáková, 2010). Parametric models describes all the component of the hydrological processes and are based on the modelling of storages (reservoirs), which are filled through fluxes such as rainfall, infiltration or percolation, and emptied through evaporation, runoff, drainage, etc (Wagener et al., 2004). Some empirical equations are used in this model and the parameters are assessed not only from field but also through calibration through curve fitting (Devi et al., 2015). Physical based model is a representation of the real-world system (Xu, 2002) and is based on the understanding of the physics of hydrological processes and are characterized by parameters that are in principle measurable and have direct physical significance (Džubáková, 2010). Devi (2015) stated that in this method, huge amount of data such as soil moisture content, initial water depth, topography, topology, dimensions of river network etc. are required but finally can provide more information on the hydrological processes.

Comparing the three model types, the mechanistic or physical-based model has the advantage of representing the spatial heterogeneity and conditions within a watershed and capacity to simulate any type of event (Ma et al., 2016; Beven et al., 1988).

2.3.1. Some examples of physically based model

MIKE SHE Model

MIKE Systeme Hydrologique Européen (SHE) model was developed in 1990 and accounts for various processes of hydrological cycle such as precipitation, evapotranspiration, interception, river flow, saturated ground water flow, unsaturated ground water flow etc (Devi et al., 2015). According to the report of Devi (2015), this model can simulate surface and groundwater movement, their interactions, sediment, nutrient and pesticide transport and various other water quality problems within a study area.

SWAT Model

Soil and Water Assessment Tool (SWAT) is a semi-distributed hydrologic model operating on a daily time step and uses a modified Soil Conservation Service-Curve Number (SCS CN) method to calculate runoff (Baker & Miller, 2013). In this model, isolating hydrologic response to a single variable (i.e land use and land cover change) is possible (Baker & Miller, 2013). Baker (2013) also added that one advantage of using SWAT is that the input data may be obtained from global public domains and is therefore beneficial in developing countries with few or scarce historical data or lack active monitoring in watersheds. The gap of this model is probably its inability to compute hourly time step which is needed in analyzing event-based flashflood.

HEC-HMS/RAS Model

Hydrologic Engineering Center's Hydrologic Modeling System (HEC-HMS) is designed to simulate rainfall-runoff processes of dendritic watershed systems (Knebl et al., 2005). It includes several options for infiltration, runoff routing, base flow and river routing (Saghafian et al., 2008) wherein maximum daily rainfall was used as input in the model and converts precipitation excess to overland flow and channel runoff (Knebl et al., 2005). HEC's River Analysis System (HEC-RAS) is a hydraulic model that simulate unsteady flow through the river channel network and requires as input the output hydrographs from HMS; its parameters are representative cross-sections for each sub basin, including left and right bank locations, roughness coefficients (Manning's *n*), and contraction and expansion coefficients (Knebl et al., 2005).

Open Limburg Soil Erosion Model (OpenLISEM)

OpenLISEM is a spatially distributed physically based model that is completely incorporated in a raster GIS which simulates hydrology and sediment transport during and immediately after a single rainfall event on a catchment scale (Kværnø & Stolte, 2012). Originally, LISEM was developed as a soil erosion model to calculate the effects of land use changes and explore soil conservation scenarios (De Roo et al., 1996). Improvements of the model were later introduced to the older version and the model was made openly available in 2011. The newer version is now able to simulate effects of detailed land use changes or conservation measures on runoff, flooding and erosion during heavy storms (http://blogs.itc.nl/lisem/, 2013).

Basic processes incorporated in the model are rainfall, interception, surface storage in micro-depressions, infiltration, vertical movement of water in the soil, overland flow, channel flow (in man-made ditches), detachment by rainfall and throughfall, transport capacity and detachment by overland flow (Jetten, 2002). Parameters and variables that are sensitive to soil conservation measures such as hydraulic conductivity, aggregate stability, raindrop energy, soil cohesion and spatial variability are also considered in the model which are necessary in analyzing the impacts of soil conservation approaches (de Barros, Minella, Dalbianco, & Ramon, 2014). Advantage of this model is the capacity to identify the physical soil and surface parameters that control the magnitude and characteristics of hydrograph and sedimentographs that reflect the degree of soil degradation within the catchment caused by anthropogenic activities (de Barros et al., 2014).

3. STUDY AREA

3.1. Location and Geomorphologic Setting

The Philippines is an archipelagic country situated at the western Pacific located within the geographic coordinates 4˚23'N – 21˚25'N latitude and 112˚E-127˚E longitude. It is bounded by South China Sea to the north and west, Celebes Sea to the south and Pacific Ocean to the east (Badilla, 2008). The country is typically characterized by rugged terrain, deep narrow valleys and extensive floodplains and is drained by 19 major river basins ("Major River Basins in the Philippines," n.d.).

Metro Manila, is the capital region of the Philippines with a population of 12.88 million in 2015 according to Philippine Statistics Office (2016). It is located at the western coast of Luzon and is bounded by Manila Bay to the west, Laguna Lake to the east, Sierra Madre Mountains to the northeast and Pampanga river delta to the northwest. A large portion of Metro Manila occupies floodplains and deltas associated with Marikina and Pasig River.

The study area is the Marikina River Basin (herein referred to as MRB) which geographically lies between 14˚33'26.14" – 14˚50'11.91" north latitude and 121˚3'39.37" – 121˚19'32.45" east longitude (Abino, Kim, Jang, Lee, & Chung, 2015) (Figure 3.1). It has a catchment area of 698.2 km² with its headwaters coming from the western slopes of Sierra Madre Mountain Range (Abon, David, & Pellejera, 2011). It is characterized by flat and low-lying areas on the western side and grades from gently rolling hills to rugged terrain towards the east. The rugged ridges are part of the Sierra Madre Mountains with its highest elevation at 1122 msl (Badilla, 2008)

Figure 3.1 Location of Marikina River Basin (Source: Google Earth)

The Marikina River floodplain is in part defined by the Valley Fault System, with the up thrown blocks comprising the high relief areas of Antipolo City to the east and the Diliman Plateau to the west (Abon et al., 2011). Several rivers, including Montalban, Wawa, Tayabasan, Boso Boso, Manga, and Nangka, feed into the 31-km Marikina River that flows southward towards Pasig River and eventually empties its load to Manila Bay.

3.2. Climate

Philippine climate is tropical and maritime, and is mainly characterized by relatively high temperature, high humidity and abundant rainfall ("Philippine Atmospheric, Geophysical and Astronomical Services Administration (PAGASA)," n.d.). Rainfall distribution throughout the country varies from one region to another, depending on the direction of the moisture-bearing winds and the location of the mountain systems (PAGASA website).

Fluctuations in rainfall is mainly attributed to the disturbances in the monsoon flow, easterly wave, Intertropical convergent zone (ITCZ), tropical cyclones, and local weather systems. On average, the mean annual rainfall of the Philippines varies from 965 to 4,064 millimeters (PAGASA, n.d).

Based on the Philippine climate classification, Metro Manila has Type I climate defined as having two pronounced seasons: dry from November to April, and wet for the rest of the year (Figure 3.2). The maximum rain period is from June to September. Historical records of climatological extremes of rainfall (1961-2015) taken from the Diliman Science Garden station show that the greatest 24-hr rainfall occurred on 26 September 2009 during the passage of Tropical Storm Ketsana (local name: "*Ondoy"*) in Metro Manila with 455.0 mm of rainfall. This record exceeded the normal monthly values for September (1981-2010) in Science Garden which is 451.2 mm. ("Philippine Atmospheric, Geophysical and Astronomical Services Administration," n.d.; Badilla et al., 2014).

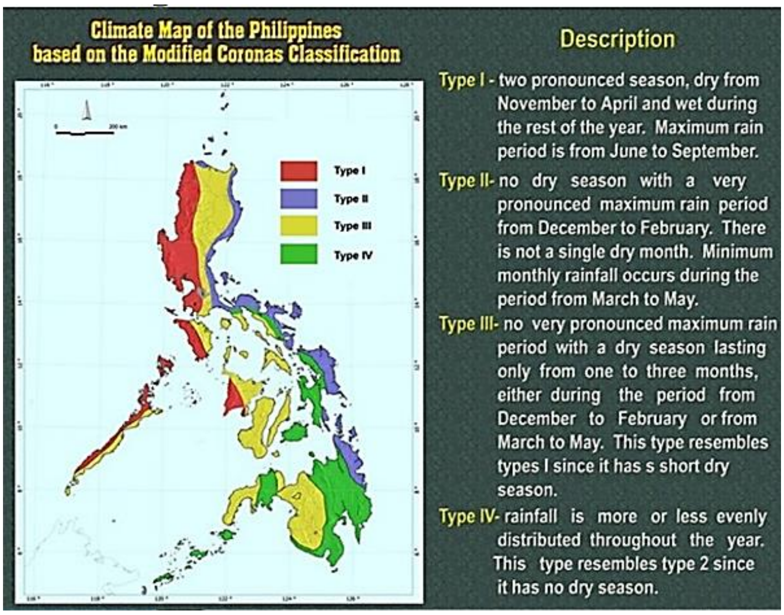

Figure 3.2 Climate map of the Philippines (Source: www.pag.dost.gov.ph)

3.3. Land use and Land cover

MRB consists of a variety of land use and land cover namely agricultural land, brushland, plantation, built-up, forest land, grassland and waterbody (Figure 3.3). The rugged terrain at the upper reaches of the catchment at the eastern ridge boundary is largely covered by thick primary and secondary forest which is part of the Marikina Watershed Reservation. The lower slopes of the western ridge, as well as the eastern slopes, are typically covered by grasslands, patches of second growth forests, patches of plantation of some

Figure 3.3 Land cover within the study area includes (a) forest, (b) shrub, (c) agriculture and (d) built-up areas

fruit-bearing trees, bananas, corn, some cash and root crops, and occasionally rice in negotiable slopes and where soil is able to support it (AECOM, 2012). Agricultural land, particularly rice fields, are sporadically located within the flat lands near natural channels and irrigation canals. Built up and commercial areas are concentrated at the central region towards the west but land development are presently progressing north-eastward. Few patches of bare land can also be noted within the rolling terrain of the catchment which are presently utilized as quarry areas.

3.4. Soil

Soil series map of the study area was available from the Bureau of Soils and Water Management (Figure 3.4). The eastern section of the catchment towards the ridge boundary is typically underlain by boulder to gravelly material which normally grades to finer particles of silty clay loam texture belonging to the Antipolo series undifferentiated. The lower hills consist of clay materials of the Antipolo and Binangonan clay series. Antipolo clay is very friable and composed of fine granular clay with the presence of spherical tuffaceous materials. The Binangonan clay is dark brown to nearly black clay, coarse granular to cloddy when dry and sticky when wet (AECOM, 2012). Flat area adjacent to Marikina River is underlain by silt loam and clay loam of the Marikina series which is a typical recent alluvial soil. Marikina silt loam principally covers the valley section of the study area. Marikina clay loam on the other hand, is found on the western side of

Marikina Valley. In the Marikina series, soils are deep, poorly drained and occurs on level to nearly level (0.0 – 2.0% slopes) minor alluvial plain (Carating et al., 2012)). Clay loam units of the Marikina, Antipolo and Bantay series are generally found in areas near Laguna de Bay while Novaliches clay loam is found near the Lamesa Watershed area. Towards the western boundary of the catchment, clay loam adobe and clay adobe of Novaliches and Guadalupe series, respectively, underlie the area. Both series are derived from volcanic tuff (Carating et al., 2012).

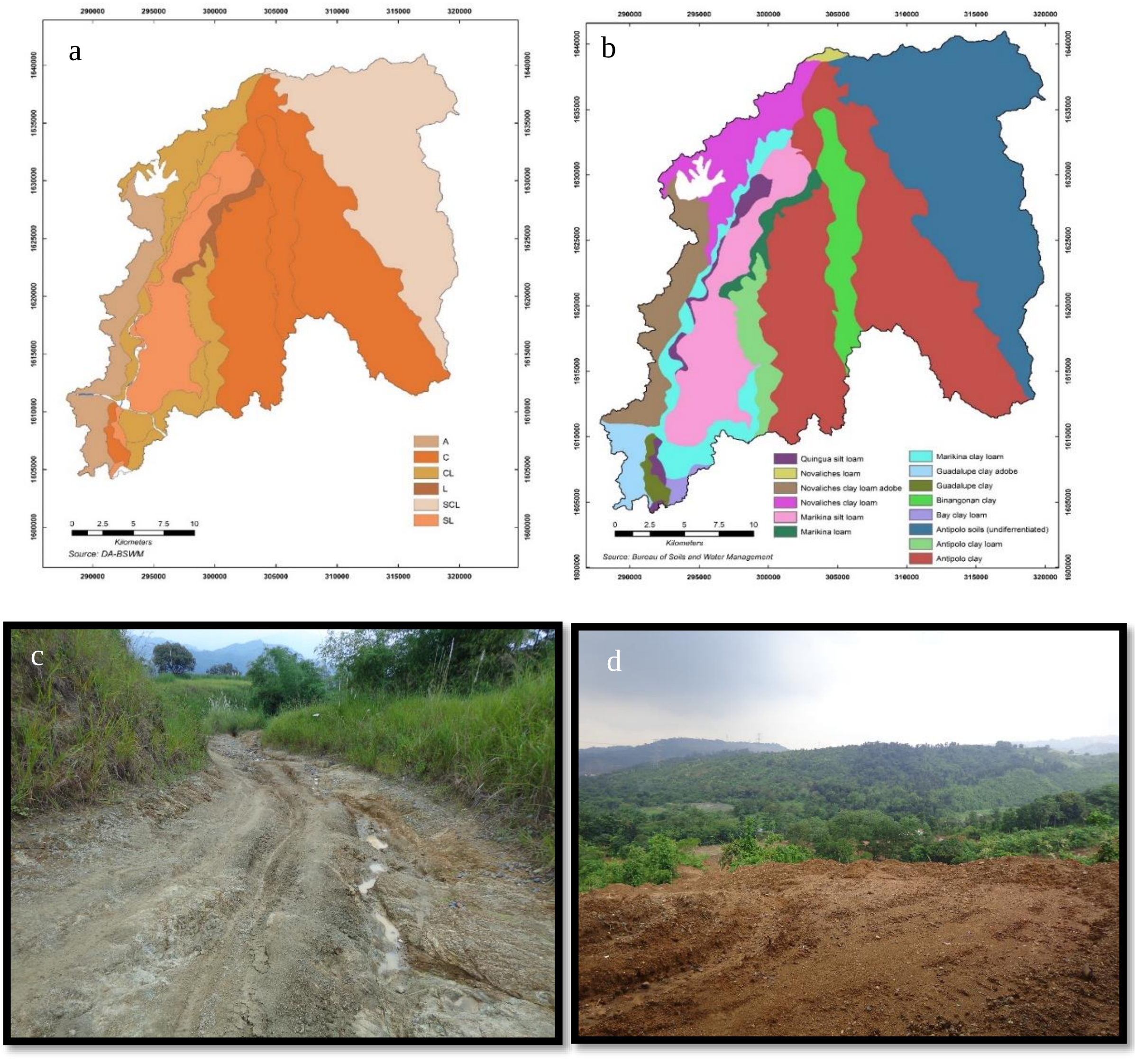

Figure 3.4 (a) Major soil texture units underlying the study area; (b) Soil series Map (Source: DA- BSWM); (c) Binangonan clay exposed along the road in Brgy. Mascap, Rodriguez, Rizal; (d) Antipolo clay underlies the northern part of Rodriguez, Rizal

3.5. Socio-Economic

3.5.1. Population

MRB is largely composed of the province of Rizal and a portion of Metropolitan Manila which covers 79% and 19% of the total area, respectively, which encompasses fifteen cities and municipalities (Figure 3.5a).

Based on the available data (NSO, 2015), population density had been rising gradually during the past 15 years, i.e., from 2000 to 2015 (Table 3.1) (Marikina River Basin Master Plan, n.d). It shows that Montalban has the highest growth rate of 15% over the past 15 year record (2000 – 2015) while Pateros has the slowest rate of 0.5% (Figure 3.5b).

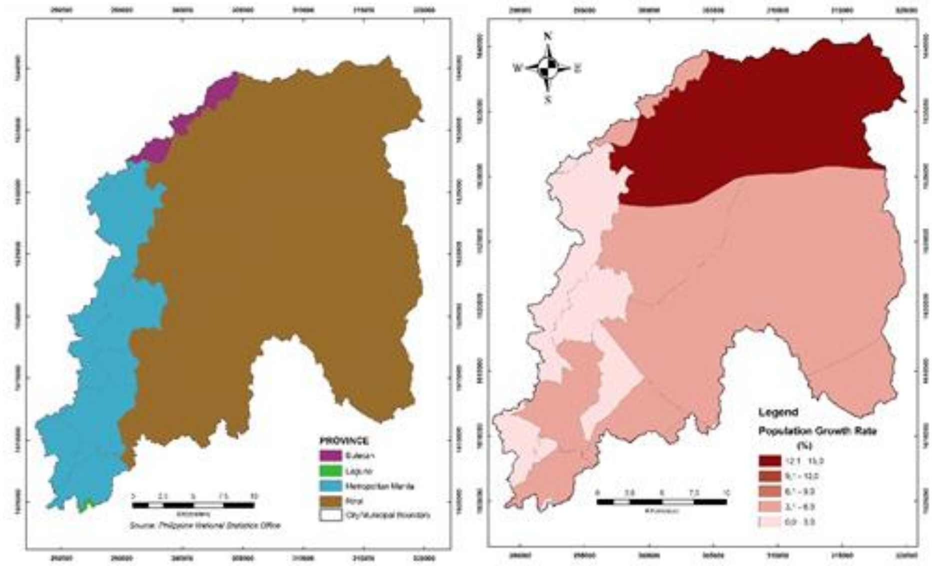

Figure 3.5 (a) Provincial boundary map of MRB; (b) Spatial distribution of growth rate in MRB

Table 3-1 Population Density and Urban Population (Source: Philippine Statistics Authority, 2000, 2010 and 2015 Census of Population)

City/Municipality	***Land Area (sq.km)***	***2000 Population ('000)***	***2010 Population ('000)***	***2015 Population ('000)***	***Population Growth Rate (%) (2000 – 2015)***
Angono	2	74.7	102.4	113.1	3.4
Antipolo	246	470.9	677.7	774.7	4.3
Cainta	17	242.5	311.8	321.4	2.2
Makati	12	444.9	529.0	579.4	2.0
Marikina	22	391.2	424.1	448.9	1.0
Pasig	31	505.1	669.8	753.0	3.3
Pateros	2	58.9	64.1	63.6	0.5
Quezon City	50	2,173.8	2,761.7	2,919.6	2.3
Montalban	182	115.2	280.9	368.7	14.7
San Jose Del Monte	12	315.8	454.5	573.4	5.4
San Mateo	57	135.6	205.2	252.1	5.7
Taguig	16	467.4	644.5	801.1	4.7
Tanay	25	78.2	98.9	116.5	3.2
Taytay	20	198.2	289.0	318.6	4.0

3.5.2. Industrialization

According to the Marikina River Basin Master Plan (RBCO, n.d.), large expanses of agricultural lands have been rapidly been converted into residential, commercial and industrial areas. The Province of Rizal has been considered as the most industrialized region in the country, where major industrial establishments are mostly resource-based (i.e. agri-business, food and beverage manufacturing, mineral products).

The industrialized areas of Rizal are the cities of Antipolo, Cainta and Taytay consisting of manufacturing establishment as well as businesses involved in woodworks, garment production and food processing. Other towns are involved in poultry, piggery and quarrying industries. In Metro Manila, industrial areas are also proliferating notably in Marikina, Pasig, Quezon City and Taguig. However, industrial land usage are is generally lessening due to its expansion outside the metropolis. Vertical development of residential units has also been the trend due to limited space.

3.6. Historical Flood

Since the 1940's, the first recorded flood event in Metro Manila, major floods have been devastating the area especially during typhoon season. In the report of Bankoff (2003), he identified some of this events to have occurred in the years 1948, 1966, 1967, 1970, 1972, 1977, 1986, 1988, 1995, 1996 and 1997. Since 2000, more extreme flooding events took place and the most damaging was in September 2009 during the passage of Typhoon Ketsana (local name TS Ondoy) (Figure 3.6). In this event, a 455.0mm rain was recorded within 24 hours in Science Garden Station which exceeded the normal monthly values (451.2 mm) for the month of September (1981 to 2010) (Badilla et al., 2014). During this occurrence, a large extent of Metro Manila particularly areas within MRB were inundated and submerged under deep flood waters. Subsequent flooding in Marikina Valley also happened in 2011, 2012 and 2013 caused by typhoon and enhanced moonsonal rains.

Figure 3.6 Devastation during the onset of TS Ondoy in 2009 (Source: http://lollitop.blogspot.nl; http://s168.photobucket.com)

4. METHODOLOGY

As mentioned in the introduction, the main objective of this research work is to evaluate the impact of land use/land cover change to run-off generation and flooding within the MRB. To attain this objective, the work was divided into two phases. First is the LULC change detection followed by the hydrologic modelling using a physically-based model.

4.1. Land Use and Land Cover Change Analysis

In order to do the LULC change analysis, it is necessary to initially determine the different land use/land cover type within the study area for the past decades which in this case, considered 1989 and 2016. This can be done by generating LULC maps using digital image classification.

Landsat imageries of the study area, acquired on April 4, 1989 and April 17, 2016, of path 116 and row 50 were acquired from USGS website (http://earthexplorer.usgs.gov/). Both the images were obtained in April indicating minimal phenological variations (Lunetta & Elvidge, 1999). Also, summer time was chosen to ensure minimal cloud cover over the area.

4.1.1. Image data processing and land cover classification

Pre-processing techniques such as radiometric calibration and atmospheric correction (Quick atmospheric correction) were applied to the obtained images. Radiometric correction is done to convert digital numbers (DN) to reflectance while atmospheric correction (QUAC) was applied in order to remove any atmospheric absorption and scattering effects. The latter is an automated atmospheric correction method applied in ENVI for retrieving spectral reflectance from multispectral and hyperspectral images (Harris Geospatial, n.d).

After pre-processing, the corrected images were exported to ERDAS for classification. Primarily, supervised signature file was created using the area of interest (AOI) tool and training samples as reference. For the 2016 image, 65 training points obtained from field and digitally were used, while 48 training points entirely obtained from google earth imagery were used to classify the 1989 image. The signature files were then applied to train the software in administering the selected classification algorithm.

Although a number of classification schemes are available, supervised classification method specifically Spectral Angle Mapper (SAM) algorithm was applied in this work. According to Kruse (1994), the simplest way to produce maps showing the spatial distribution of specific materials is to empirically match image spectra to reference spectra such as the SAM algorithm. The algorithm determines the similarity between two spectra by calculating the "angle" between an unknown spectrum to one or more reference spectra (Figure 4.1), treated as vectors in a space with dimensionality equal to the number of bands (n) as shown in equation (1) (Kruse, 1994; Addamani, 2014; Shafri et al., 2007; Dennison et al., 2004).

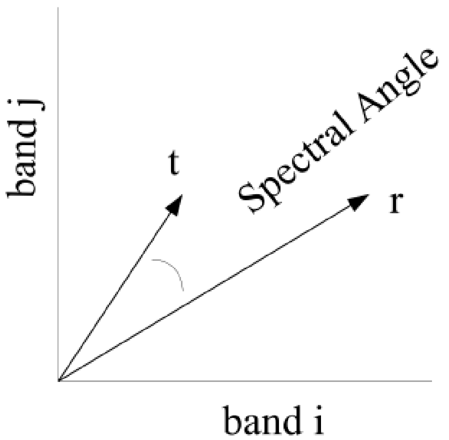

Figure 4.1 SAM algorithm representation (ITC, 2016)

$$SA = \cos^{-1}\left(\frac{\sum_{i=1}^{n} t_i r_i}{\sqrt{\sum_{i=1}^{n} t_i^2 \sum_{i=1}^{n} r_i^2}}\right)$$

where: n : number of bands
t : pixel spectrum
r : reference spectrum
SA : spectral angle **(1)**

Smaller angles denotes closer matches to the reference spectrum (Shafri et al., 2007). This algorithm is adopted in this research work as it is considered as a very powerful classifier because it is not affected by solar illumination factor and also contains the influence of shading effects to highlight the target reflectance characteristic (Moughal, 2013).

Additional steps were also undertaken in ARCGIS to improve the classified image. Conditional statements were generated to incorporate a priori knowledge about the study area using information on elevation (DEM) and slope (e.g. *Con((iff 2016 classified image=agriculture & (DEM>200), forest, 2016 classified image)*. Finally, 3x3 major filtering was also performed to both images to remove isolated pixels or noise. After this, accuracy assessment was carried out using 48 and 40 test pixels collected during fieldwork and digitally, for the 2016 and 1989 classified image, respectively, as presented in chapter 5.

4.1.2. Land cover/land use change analysis

Once the independently classified image of 1989 and 2016 LULC maps are prepared, the work proceeds to detecting land use/land cover change which is an integral part of this research work in order to establish a relation and better understanding on the influence of different land cover types to overland flow generation. Changes can either be triggered naturally or anthropogenically. In this present work, the observed changes will be correlated to the socio-economic factor that could have influence such changes.

In this study, the post classification approach was used to analyse the changes of land cover types in MRB. Post classification comparison technique is the most widely used method for change detection as there is no need for co-registration of images involved, it has low sensitivity to spectral variation and provides a "from-to" change information (Raja et al., 2013). Emphasis was given to the significant change of forest cover in the upper reaches of catchment and of built-up areas in the lower portion wherein there was a substantial decrease and increase, respectively between 1989 and 2016. The change detection analysis was implemented in ERDAS Imagine with the use of change matrix tool.

4.2. Data Collection and processing

4.2.1. *Fieldwork*

A three-week field activity was undertaken from September 16 to October 9, 2016 to collect primary and secondary data such as soil samples, ground truth data for image classification, hydrometeorological data and other research-related maps and documents. Coordination was initially done with colleagues from the University of the Philippines-Diliman to get preliminary information as basis for field survey within the study area. Soil core samplers and Global Positioning System (GPS) unit were the basic instruments used in the field. In addition, ancillary information were also obtained from various institution and government agencies to supplement the data needed for this research work.

4.2.2. *Rainfall Data Analysis*

PAGASA, the National Weather Bureau of the Philippines, provided data on annual maximum 24-hr rain for the period 1996-2015, measured at the Science Garden Rain Gauge Station (Appendix A). From this information, return period of extreme rainfall were calculated using the Gumbel distribution. The plot (Figure 4.2) shows that Typhoon Ketsana has the highest return period, thus the hourly rainfall data measured from four rain gauging station within the study area were used for the simulation (Figure 4.3).

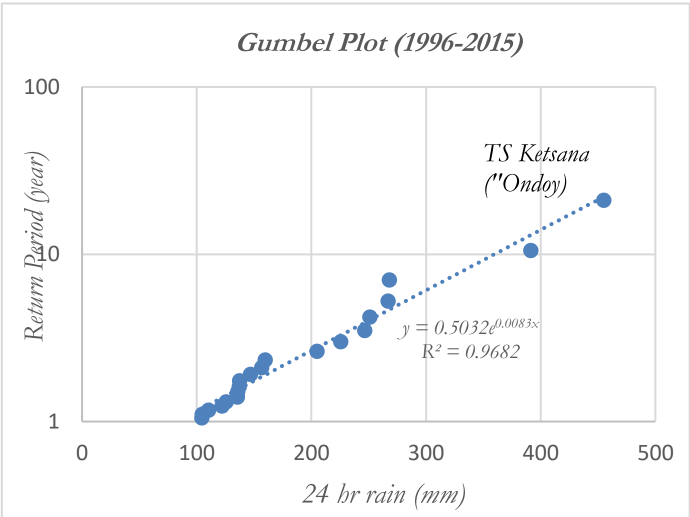

Figure 4.2 Gumbel plot of the annual max 24-hr rain

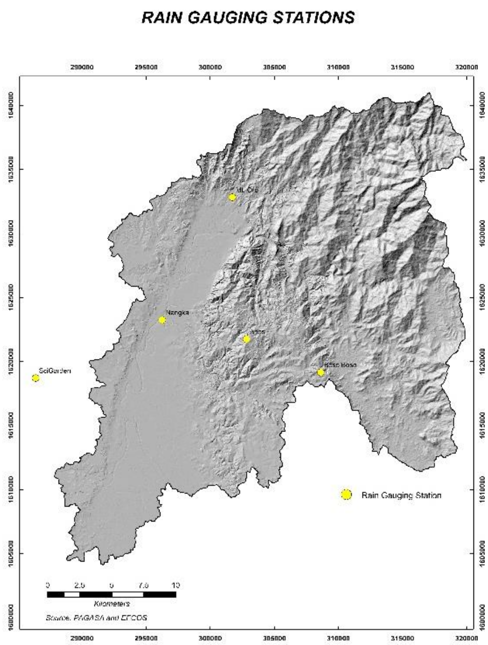

Figure 4.3 Location map of rain gauging station of PAGASA and EFCOS

Apart from using measured rainfall data of the specific rain event of Typhoon Ketsana, design storms were generated for simulating the hydrologic processes in the study area to evaluate its response to different intensities of various storm return period. Utilization of design storms in a particular rainfall-run off model may contribute largely to flood management and land use or mitigation plans. In this work, 5-, 10- and 20-year design storms were generated using the intensity-duration-frequency (IDF) relationships, based on a 41 years of rainfall record (1969 – 2010) from the Science Garden Rain Gauging Station in Diliman, Quezon City (Table 4.1).

Table 4-1 24 hours-RIDF data from Science Garden Rain Gauge Station, Diliman, QC (Source: PAGASA)

Computed Extreme Values (in mm) Precipitation									
T (yrs)	10 min	20 min	30 mins	1 hr	2 hrs	3 hrs	6 hrs	12 hrs	24 hrs
2	23	33.4	41.2	55.5	76.7	90.3	117.4	136.3	156
5	31.4	45.5	57.6	81.8	113.2	135.7	185.1	216.1	243.1
10	37	53.6	68.5	99.3	137.5	165.8	229.9	268.9	300.7
15	40.1	58.1	74.6	109.1	151.1	182.7	255.2	298.8	333.3
20	42.3	61.3	78.9	116	160.7	194.6	272.9	319.6	356
25	44	63.7	82.2	121.3	168.1	203.8	286.5	335.7	373.6
50	49.2	71.2	92.4	137.6	190.8	231.9	328.5	385.2	427.6
100	54.4	78.7	102.5	153.8	213.3	259.9	370.2	434.4	481.2
Equivalent AVERAGE INTENSITY (mm/hr) of Computed Extreme Values									
T (yrs)	10 min	20 min	30 mins	1 hr	2 hrs	3 hrs	6 hrs	12 hrs	24 hrs
2	138	100.2	82.3	55.5	38.3	30.1	19.6	11.4	6.5
5	188.4	136.6	115.2	81.8	56.6	45.2	30.8	18	10.1
10	221.8	160.7	136.9	99.3	68.7	55.3	38.3	22.4	12.5
15	240.7	174.2	149.2	109.1	75.6	60.9	42.5	24.9	13.9
20	253.8	183.8	157.8	116	80.4	64.9	45.5	26.6	14.8
25	264	191.1	164.4	121.3	84	67.9	47.7	28	15.6
50	295.3	213.6	184.8	137.6	95.4	77.3	54.7	32.1	17.8
100	326.4	236	205	153.8	106.7	86.6	61.7	36.2	20.1

Alternating block method was used to generate the design storm hyetograph derived from the IDF curves (Figure 4.4). Given the duration and intensity, precipitation depth (mm) was consequently calculated using the formula, $P = I*T_d$, where I is the intensity (mm/hr) and T_d is the duration (hr). Incremental rainfall is then computed by taking the differences between successive precipitation depth values and used to calculate the intensities for each time-step. A design intensity hyetograph in 10-min increments for a 4 hour-storm was generated by reordering the incremental intensity blocks in a symmetrical format on the time axis with the maximum at the middle (Figure 4.5)(Olivera, Stolpa, Assistant, & Manager, 2002).

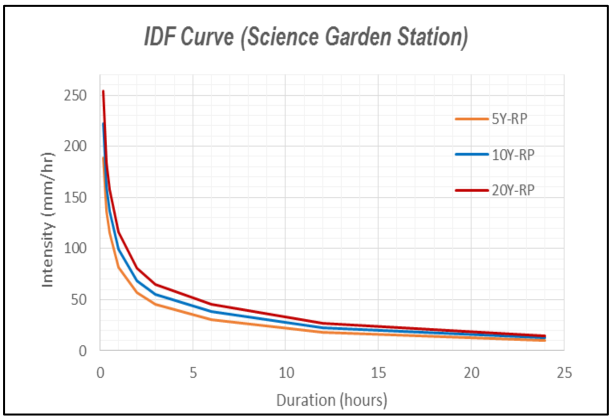

Figure 4.4 Intensity-Duration-Frequency Curves of the Science Garden Station

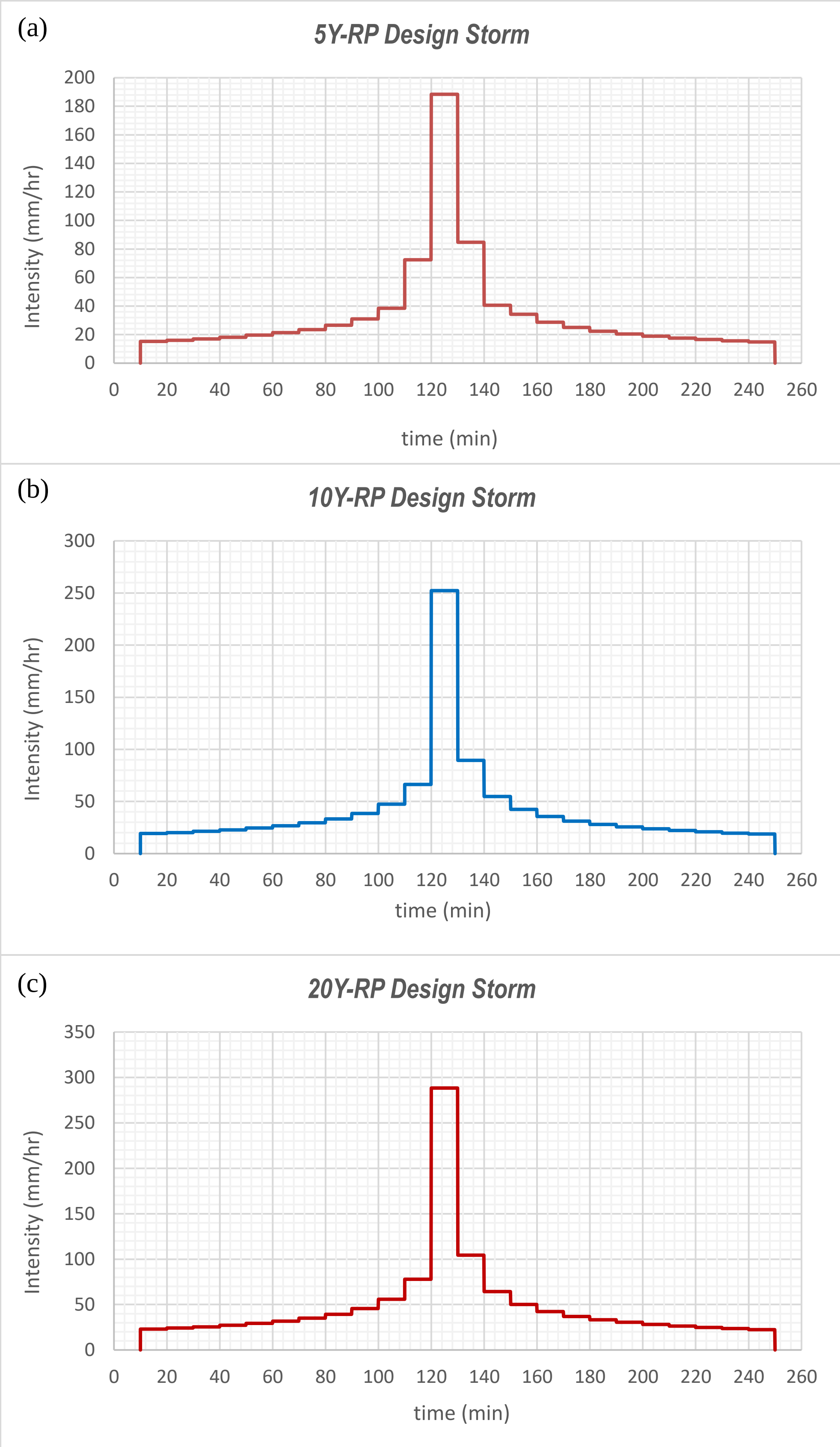

Figure 4.5 Design hyetographs of the Marikina River Basin for (a) 5y-return period; (b) 10y-return period and (c) 20y-return period

4.2.3. Digital Elevation Model (DEM) Generation

Two sets of digital elevation data were used in this study: 1-m resolution LiDAR DEM, provided by the National Mapping and Resource Information Authority (NAMRIA) and 30 m SRTM DEM, acquired from USGS website (https://earthexplorer.usgs.gov/). The LiDAR elevation data only covered the lower part of the catchment (Figure 4.6a) while SRTM DEM has a full coverage of the study area.

To keep the significant information within the floodplain from LiDAR, a mosaic of the both DEMs was used for this research work. LiDAR DEM was initially resampled to 30-meter resolution using bilinear interpolation in ArcMap that uses the distance-weighted average of four nearest pixel values to estimate a new pixel value. This interpolation method leads to smoother images and represent topography with gradual change (ITC Core Book, 2012). After resampling, both DEM (LiDAR and SRTM) were stitched together by means of mosaic tool in ArcGIS to cover the whole watershed area (Figure 4.6b). Margin of the mosaic image was examined for any abrupt changes that may affect the simulation.

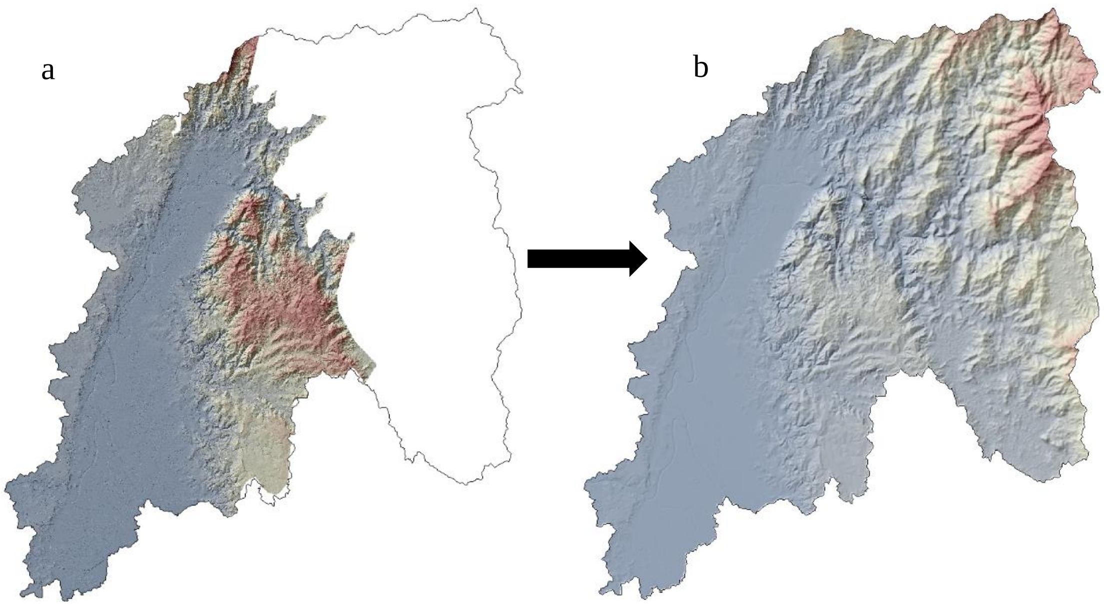

Figure 4.6 (a) 1-m resolution LiDAR DEM; (b) Mosaic of resampled LiDAR DEM with 30-m SRTM

Furthermore, infrastructures such as roads, dikes and embankments also play a significant role during flood events by influencing overland flow routes. To retain information of these features, vector file of road networks and dikes/levees particularly within the floodplain were obtained from Open Street Map (OSM) and Google Earth image. The vector file (polyline) was converted to 1-m resolution raster and then to points which correspond to each 1-m pixel of LiDAR DEM (Figure 4.7a). Elevation data of each point was extracted from the LiDAR DEM using a spatial analyst tool in Arcmap (extract values to points). This was followed by final conversion to raster dataset and resampling to 30-meters wherein cell value assignment was based initially on the maximum/minimum value of the elevation attributes of the points within the cell (Figure 4.7b).

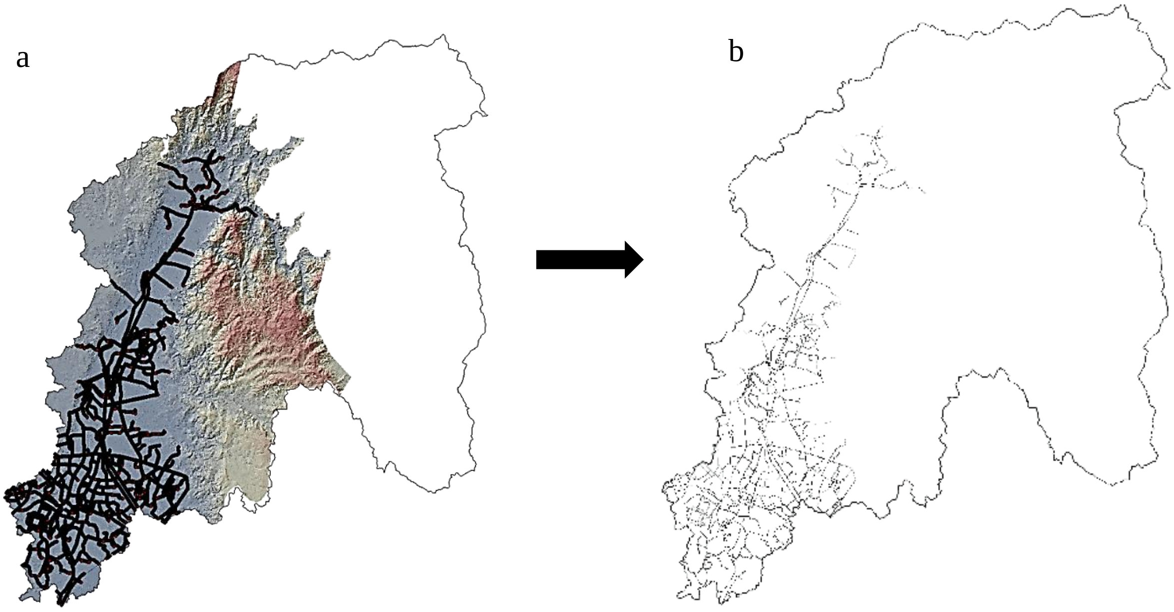

Figure 4.7 (a) Point vector of roads, dike, levees, etc overlaid onto LiDAR DEM; (b) 30-m raster layer of infrastructure features;

Similarly, river channel elevation is equally important for the model simulation. As LiDAR DEM is not accurate on areas with water such as rivers, channel bed elevation was extracted from the available channel cross sections of Marikina and Pasig River (HECRAS format) from previous studies conducted by PhilLiDAR (UPD TGACP) (Figure 4.8). The stream raster was generated by integrating the channel elevation of points extracted from the cross sections (Figure 4.9a) to the vector polygon of Marikina and Pasig Rivers (Figure 4.9b) using the interpolation method - inverse distance weighted (IDW) technique and automatically resampled to 30-m resolution (Figure 4.9c).

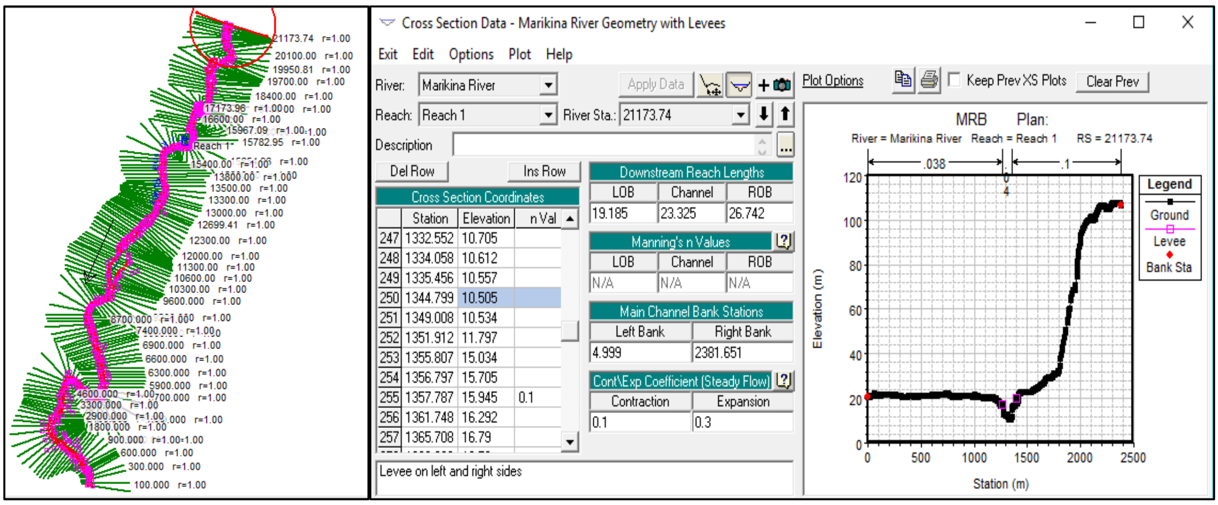

Figure 4.8 River cross section of Marikina River in HECRAS format

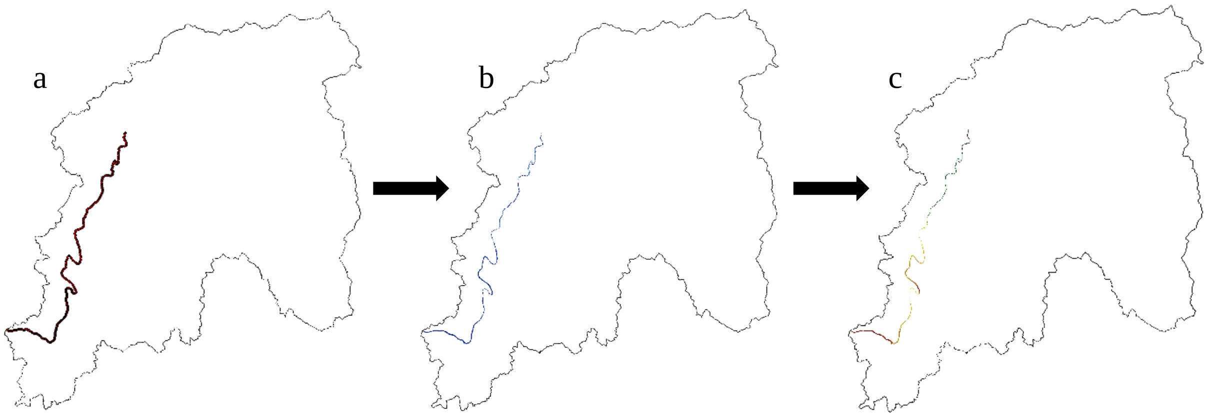

Figure 4.9 (a) point vector of channel elevation extracted from cross section; (b) digitized river channel of Marikina and Pasig river; (c) 30-m resolution stream layer with interpolated channel bed elevation

Ultimately, the final DEM was created by incorporating the Mosaic DEM with the infrastructure and main channel raster layer using cell statistics in Arcmap (Figure 4.10). This tool calculates a per-cell statistics from multiple rasters. In this case, maximum and minimum cell statistics were used for the integration of infra layer to DEM and minimum cell statistics for the main channel elevation.

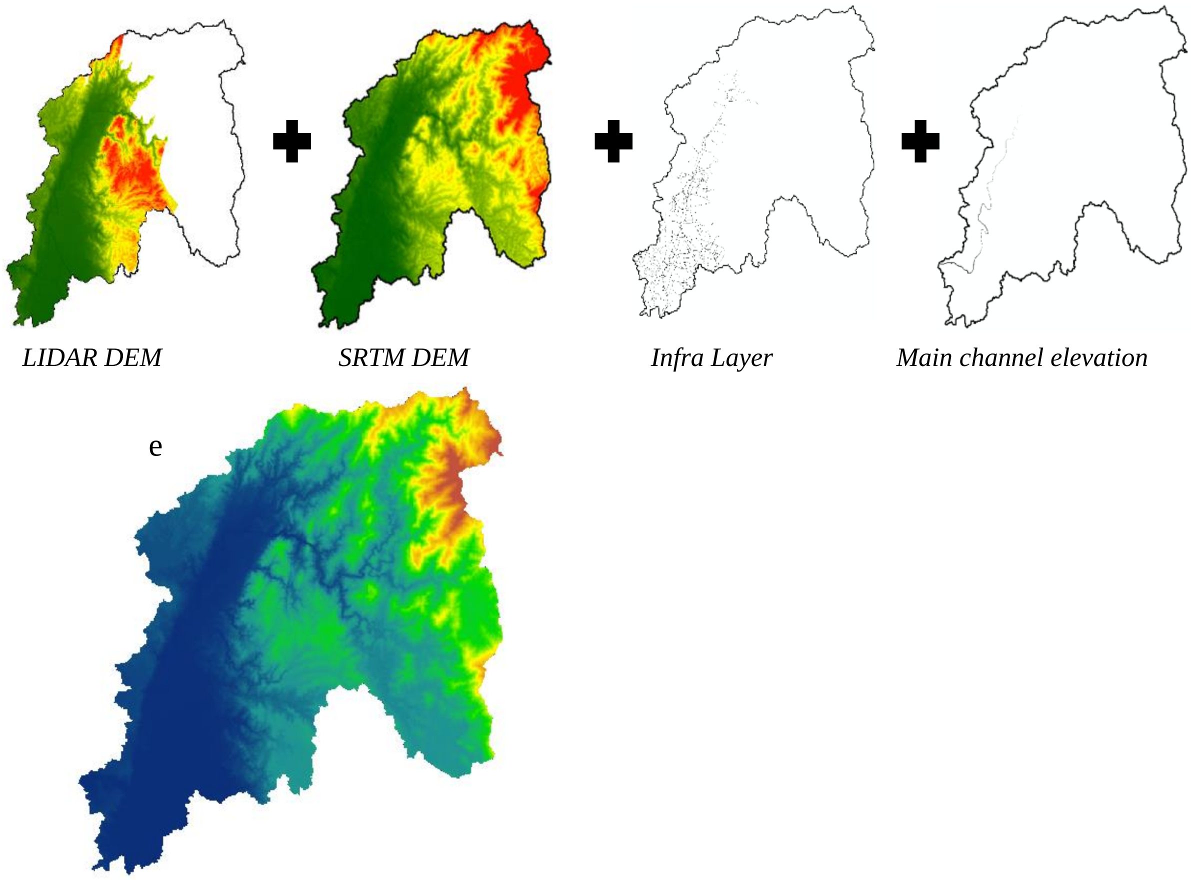

Figure 4.10 Final Digital Elevation Model (DEM) generated from the integration of LIDAR, SRTM, road/dikes and channel depth from cross sections

4.2.4. Soil data analysis

Published soil texture and soil series maps covering the whole country were readily available at the Department of Agriculture – Bureau of Soils and Water Management (DA-BSWM) from which information of the study area was extracted. Moreover, soil physical properties of various soil series area such as saturated hydraulic conductivity (Ksat), bulk density and soil texture were also gathered from the same agency.

Based on the provided soil data, twenty four (24) undisturbed samples were gathered from accessible areas in the field which will represent the different soil types. Soil sampling was done using the stratified sampling approach wherein sampling point locations were based on the soil texture units (Figure 4.11).

Figure 4.11 (L - R) Undisturbed soil sampling; Identification land cover training data; sheet flooding during the fieldwork

Analysis was done in ITC Geoscience laboratory which includes measurement of saturated hydraulic conductivity, bulk density, soil moisture and soil texture. Initially, the 24 samples were weighed to get the approximate initial moisture content and were fully saturated for 24 hours in a water tub as required by the method.

In determining saturated hydraulic conductivity of the samples, a laboratory permeameter was utilized using the constant water head method. Darcy's Law is used to calculate the K-factor in this type of method to determine permeability (Operating Instructions Manual) (2).

$$V = K * i * A * t \qquad\qquad K = \frac{V * L}{A * t * h} \tag{2}$$

Where: V = volume volume of water flowing through the sample (cm^3)
K = permeability coefficient or "K-factor" (cm/d)
i = permeability rise gradient, or: h / L (-)
A = cross-section surface of the sample (cm2)
t = time used for flow through of water volume V (d)
(d = time dimension day)
L = length of the soil sample (cm)
h = water level difference inside and outside the ring holder or sample cylinder (cm)

Textural analysis for 7 samples and 5 duplos was carried out to verify the textural identification of the representative selected samples according to the existing soil map. Primarily, the samples were oven dried for 24 hours and sieved to remove particles >2mm which was then weighed to determine its percentage within the sample. After the removal of larger particles, ~20 g fine earth materials was taken from the sieved fraction and was pre-treated to ensure complete dispersion of the primary particles. The pre-treatment stage entailed removal of organic matter and cementing materials such as calcium carbonate through oxidation. Sand-size particles were then sieved out using a 50μm sieve while the remaining silt and clay were further analyse using pipette method to determine fractions of <50 μm (silt), <20 μm (silt) and <2 μm (clay). Determination of sand fractions was obtain through sieving using mesh sizes from 1000 μm to 50μm. Finally, calculation was done to all the oven dried fractions using the formula given in the manual provided by ITC (Appendix B). Organic matter content was also determined using the Walkley Black method or by careful ashing & weighing (ITC Particle Size Analysis Manual) (Figure 4.12).

Figure 4.12 (left to right) Laboratory permeameter used for Ksat determination; Pipette analysis for fine particle size determination; sieving machine for sand-size particle determination (Source: ITC Laboratory Manual)

4.3. Rainfall-runoff-flashflood modelling

For rainfall-runoff modelling OpenLISEM was selected to simulate different scenarios. It is an open source model which can simulate soil erosion and run-off during and immediately after a rainfall event (Baartman et al., 2013). Moreover, as it is a physically-based hydrologic and erosion model, parameters can be accustomed to the existing condition of the study area. For this research, only the rainfall runoff is given focus, thus the soil erosion part of the model was disregarded. Processes that were incorporated in the model include rainfall, interception, infiltration, surface storage, overland flow, channel flow and water discharge (Figure 4.9). This model works by computing rainfall and interception by vegetation in each raster grid cell according to the input maps considered. Subsequently, infiltration and surface storage are subtracted to give the net runoff and water routing to the outlet point is based on the kinematic wave principle (Jetten, 2002). OpenLISEM operates at a catchment scale and is completely incorporated in a raster Geographical Information System (GIS) – PCRaster (De Roo et al., 1996).

4.3.1. Data preparation

OpenLISEM requires numerous basic input maps and data to better represent the catchment condition (Figure 4.13). Initially, all input database such as DEM, soil map, LULC maps, outlet map, outpoint map, road map, NDVI map, boundary map, barrier map, etc were initially prepared in ERDAS Imagine and ARCGIS interface and resampled to 30-m cell grid size. All of the raster maps were converted to ASCII format and imported to PCraster where the final OpenLISEM input database will be generated using a revised script for final conversion to the format required by the model (Appendix C).

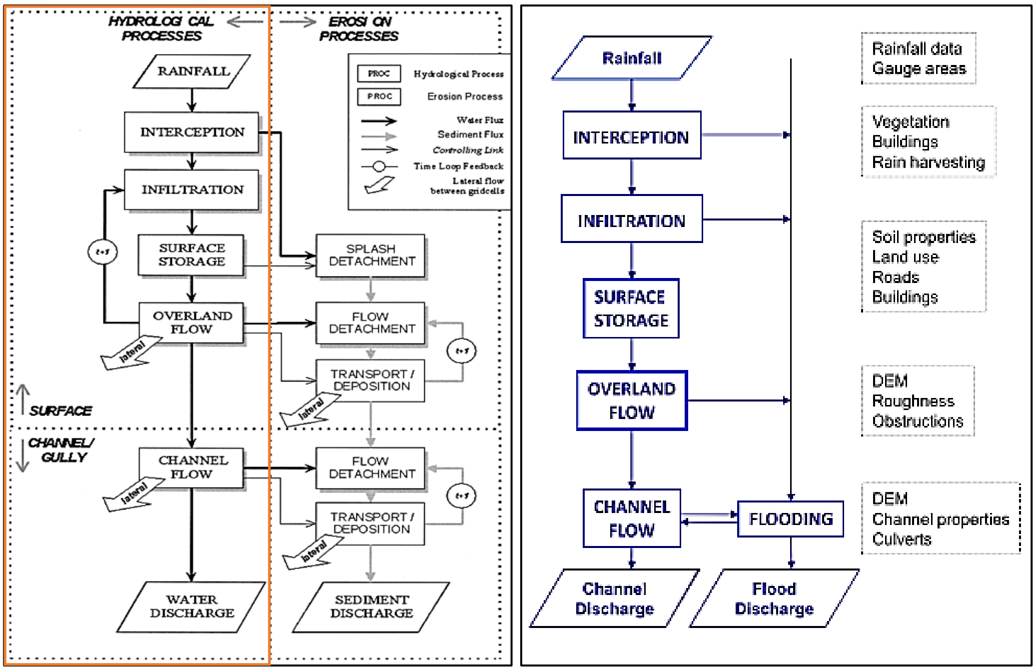

Figure 4.13 (Left) Flow chart of LISEM Model (adapted from De Roo & Jetten, 1999); (Right) General data requirement for OpenLISEM (Jetten & Shrestha, 2016)

Rainfall

Essentially, high temporal event-based rainfall data in a time series format is needed. On the other hand, for the design storm generation, intensity-duration-frequency data is required. In addition, location of rain gauges where rainfall data was measured is necessary to delineate the rain zone (refer to Figure 4.3). To take into account the rainfall spatial variability within the watershed, rainfall map for scenarios 1 and 2 was generated using Thiessen polygons method in interpolating data from the four meteostations (Aries, Boso-boso, Mt. Oro and Nangka Stations). On the contrary, for scenarios 3 to 5, it was assumed that the whole catchment will have an equal rainfall distribution using the design storm generated from one rain gauge station (Science Garden Station) (Figure 4.14).

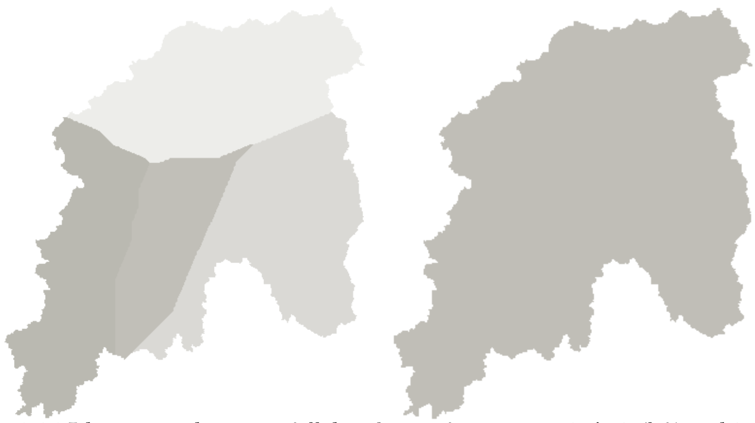

Figure 4.14 Id map to indicate rainfall distribution for scenarios 1 & 2 (left) and 3 - 5 (right)

For every time increment during the simulation of a storm, the model generates a map with the spatial distribution of the rainfall intensity using a single statement that uses the rain gauge identification map and the time series file. Thus, the model allows for spatial and temporal variability of rainfall (De Roo, Wesseling, & Ritsema, 1996).

Interception

The first process that happens with rainfall is interception by the canopy of natural vegetation and crops. For this, vegetation/crop maps were prepared initially by determining the cover fraction (C) (Figure 4.15) from the normalized difference vegetation index (NDVI) (Knijff et al., 1999). Leaf area index (LAI) (Figure 4.16) is then derived from cover fraction which is used to calculate the maximum storage capacity (SMAX) (Figure 4.17). The variables mentioned were calculated using the following equations as shown in Table 4-2.

Table 4-2 Equations used in deriving interception variables

Variables	***Equation***
Normalized Difference Vegetation Index	$NDVI = \frac{(NIR - Red)}{(NIR + Red)}$
Cover Factor	$C = 1 - \exp^{(-\alpha * NDVI)/(\beta - NDVI)}$ where α,β are parameters that determine the shape of the NDVI curve which in this case an α-value of 2 and β-value of 1.5 were used
Leaf Area Index	LAI = ln(1-C)/-0.4
Maximum Storage Capacity	Smax (Forest) = 0.2856 * LAI Smax (Shrub) = 0.1713 * LAI Smax (Grass) = 0.912 * ln(LAI) + 0.703 Smax (Crops) = 0.935+0.498 * LAI-0.00575 * $(LAI)^2$

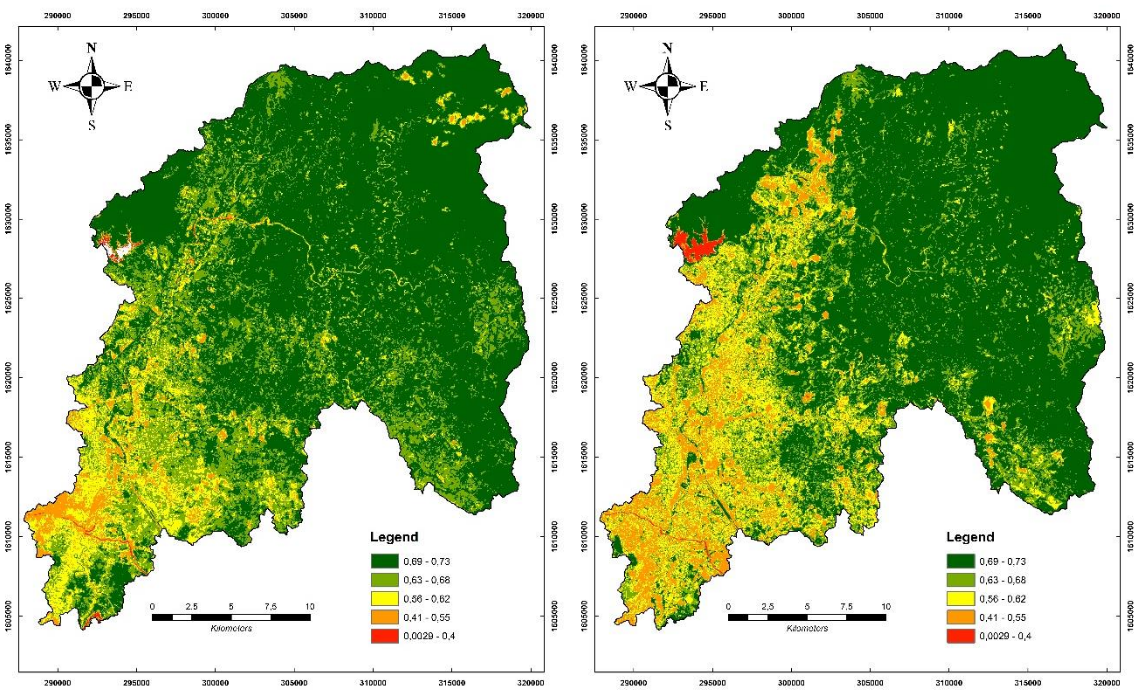

Figure 4.15 Vegetation cover fraction in 1989 (left) and 2016 (right) calculated based on NDVI

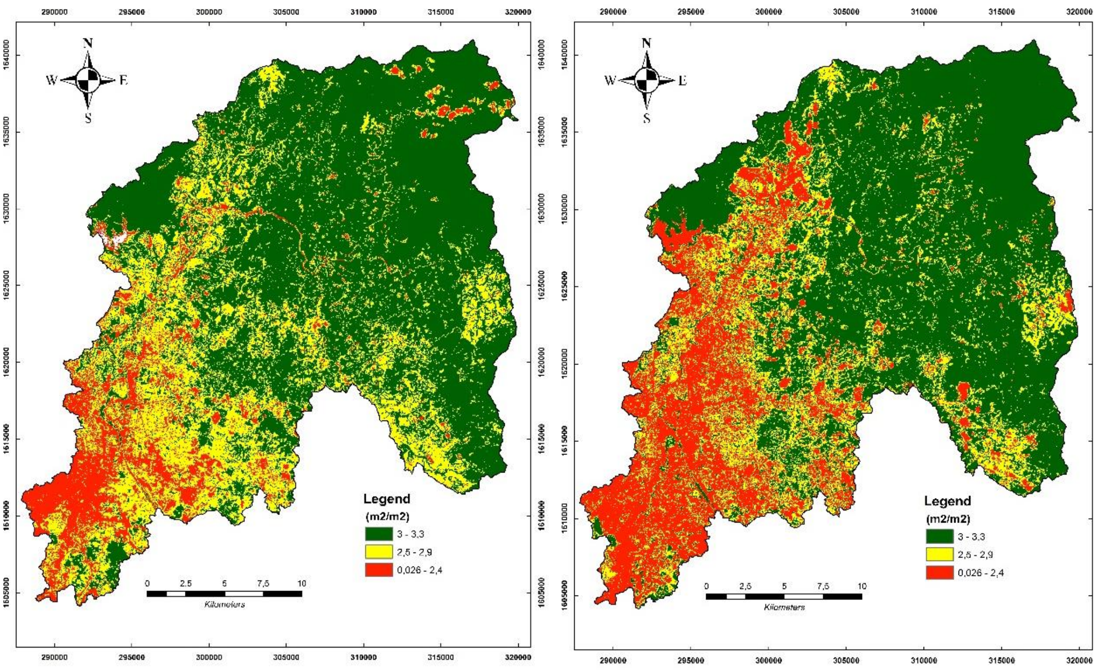

Figure 4.16 Leaf area index (LAI) in 1989 (left) and 2016 (right)

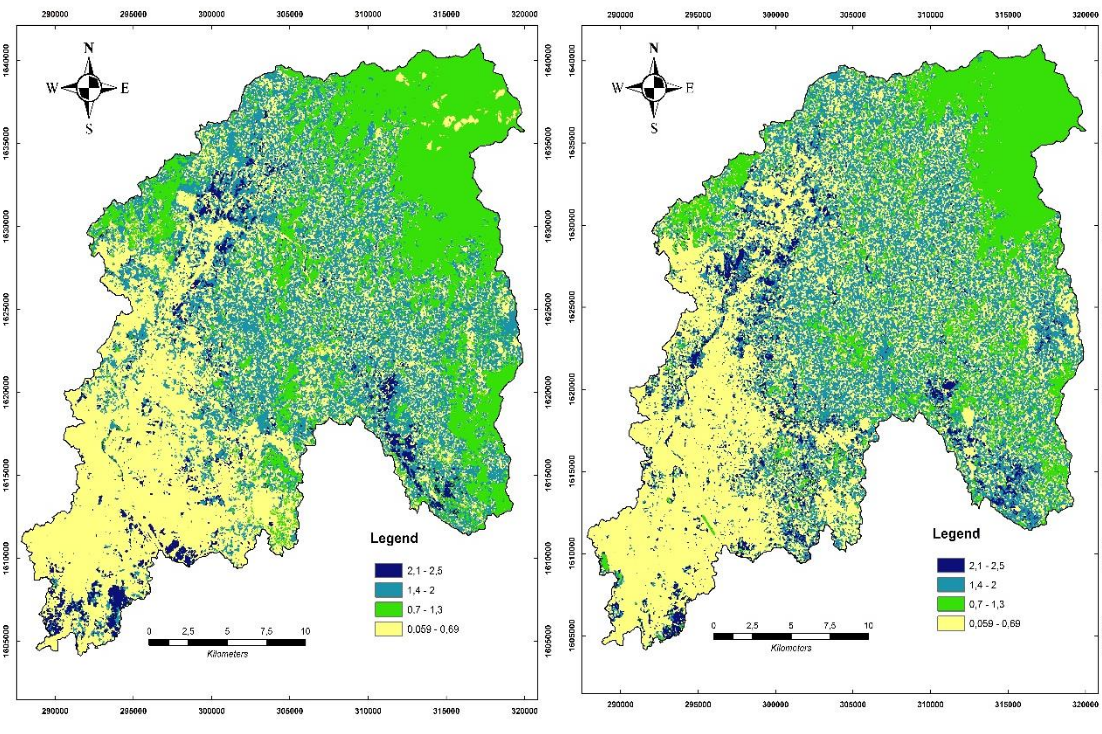

Figure 4.17 Interception storage capacity (Smax) in 1989 (left) and 2016 (right)

Infiltration and Surface Storage

Part of the rainfall not intercepted by canopy either infiltrates to the soil or stored at the surface. The rate of infiltration depends largely on soil physical properties and land use/land cover. This is simulated by OpenLISEM using the Green and Ampt infiltration equation which describes how water enters the soil from a simple application of Darcy's law (Van Mullem, 1991) (3).

$$f = K_{sat}\left(\frac{dh}{dz} + 1\right) \quad (3)$$

Where f = surface infiltration rate
K_{sat} = saturated hydraulic conductivity
dh = suction exerted by the soil
dz = distance from the surface over which the suction is applied
1 = gravity (constant)

These parameters are all inherent to the underlying soil within the study area, thus information on physical soil characteristics (Ksat, porosity, initial moisture, wetting front suction and texture) are vital. In this work, values for the mentioned parameters were obtained from laboratory results supplemented by published data of the Department of Agriculture - Bureau of Soils and Water Management and other related literature (Rawls et al., 1983) (Table 4.3). The following parameters were basis for the generation of the infiltration-related maps such as Ksat map, saturated volumetric soil moisture content map, initial volumetric soil moisture content map and soil water tension at the wetting front map.

Table 4-3 Soil physical parameter values

Texture	Bulk Density (g/cm^3)	Porosity	Ksat (mm/hr)	Initial Soil Moisture	Wetting Front Suction (cm)
Novaliches Loam	1.25	0.53	3	0.20	8.89
Novaliches Clay Loam	1.25	0.53	3	0.20	20.8
Antipolo Soil (undiff)	1.52	0.43	43	0.29	27.3
Antipolo Clay	1.3	0.51	0.43	0.34	31.6
Binangona Clay	1.35	0.49	0.1	0.22	31.6
Marikna Clay Loam	1.25	0.53	3	0.16	20.8
Marikina Silt Loam	1.3	0.51	0.64	0.33	16.6
Marikina Loam	1.45	0.45	4.6	0.19	8.9
Novaliches Clay Loam Adobe	1.48	0.44	9.9	0.19	20.8
Quiangua Silt Loam	1.3	0.51	12	0.14	16.6
Antipolo Clay Loam	1.4	0.47	12	0.26	20.8
Guadalupe Clay Adobe	1.48	0.44	9.9	0.20	4.9
Guadalupe Clay	1.28	0.51	0.61	0.25	31.6
Bay Clay Laom	1.25	0.53	3	0.27	20.8

Also, hard surfaces such as roads affect infiltration of water. In this model, road layer was acquired from openstreet map and classified into primary, secondary and tertiary roads. The width of each section were approximate measurement based from google earth image ranging from 3 meters to 30 meters (Figure 4.18).

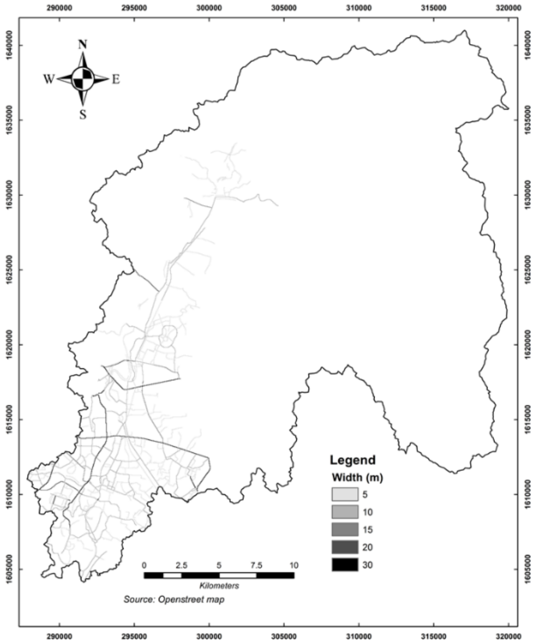

Figure 4.18 Road layer map showing road width in meters

Overland Flow

When infiltration and saturation is exceeded, overland flow (surface runoff) is generated. Runoff velocity and flow direction vary spatially and is mainly determined by the terrain conditions which also defines the channel network. Likewise, surface roughness expressed by Manning's n and random roughness (rr) also influence the flow of runoff and this value differs depending on land cover type (Table 4.4). Manning's n values of the existing land cover types in the area were obtained from literature (Chow, 1959).

Table 4-4 Land cover type parameters that influences runoff velocity

Land cover type	***Plant height***	***Random Roughness (RR)***	***Manning's n***
Forest	20	1.5	0.1
Shrub	3	1.5	0.1
Grass	1	1.5	0.035
Agriculture	0.5	1.8	0.035
Built-up	0	0.7	0
Water body	0	0	0

Channel Flow

Data required in this part include DEM which is used to derive input maps such as the local drain direction map (ldd). The ldd map gives each cell the direction of runoff towards the channel network. The channel network was defined by using OSM data, however, channels at the lower catchment were modified in ARCGIS by adjusting the polylines based on the LIDAR DEM (Figure 4.19). In addition, channel width was also approximated from the LIDAR DTM. On the other hand, to define channel properties, constant values were considered in the calculation such as channel cohesion, Manning's n value of channel, channel side angle, channel saturated hydraulic conductivity and minimum slope (Table 4-5).

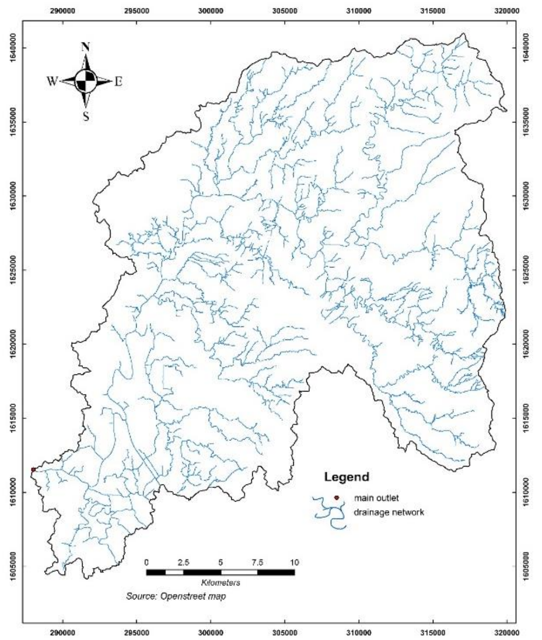

Figure 4.19 Channel work of the study area

Table 4-5 Constant values used to define channel properties

Property	Value
Channel cohesion (kPa)	8
Channel Manning's n	0.04
Channel side angle	0
Channel Ksat	1
Minimum slope	0.002

Water Discharge

To provide location points of measurement for the model simulation, three outpoints were defined in this work (Figure 4.20). Outpoint 1 is located at the base of the upper catchment as to differentiate the influence of land cover changes upstream in terms of discharge and water level along the channel. Outpoint 2 is located at the flood plain section while outpoint 3 is the main outlet and is located at the eastern edge of the watershed boundary.

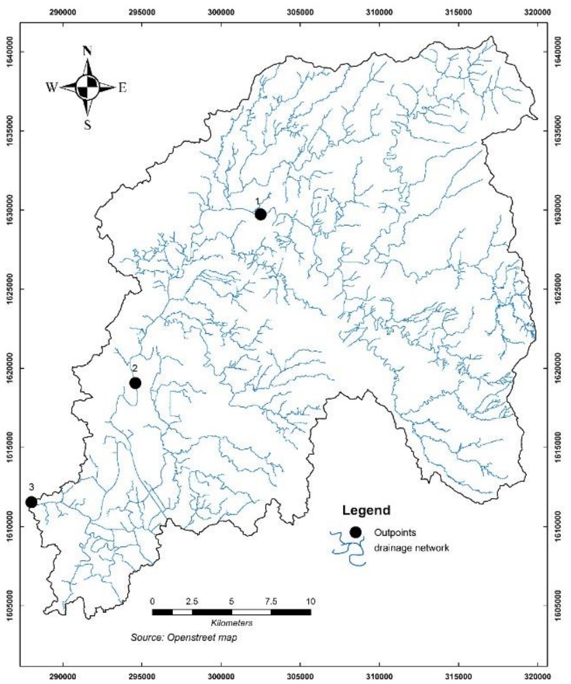

Figure 4.20 Location of outpoints

4.3.2. Flood Model Development

Once all input maps and rainfall table are prepared, these are then inputted to OpenLISEM interface. For the simulation, the run file used is luse50m.run which contains all the options and map names of a single run whereas the rainfall file selected depends on the scenario being simulated.

Primarily, flood simulation was carried out using the rainfall data of Typhoon Ketsana in 2009 and 2016 database. For this, hourly data from four (4) rain gauging stations (Aries, Boso-boso, Mt. Oro and Nangka Stations) within the catchment was provided by Metro Manila Development Authority – Effective Flood Control Operation System (MMDA-EFCOS) (Refer to Figure 4.3). The 42-hours rainfall which covered the duration from September 25 (1400H) to September 27 (0800H) was specifically used in the simulation. The results of the initial run was then calibrated by comparing simulated water level with measured water level at Sto. Niño gauging station. Once satisfied with the calibration result, the modified parameters will then be utilized in running the model for the simulation of flood event using the 1989 database.

Additionally, 5-, 10- and 20-year return period rain events generated from Intensity-Duration-Frequency (IDF) curves were also used in simulating flood scenarios. IDF Curves are derived from the statistical frequency analysis of rainfall records over a period of time (Subyani & Al-Amri, 2015), which in this case is 1969-2010, measured from one gauging station (Science Garden Station) in Diliman, Quezon City operated by the Philippine Atmospheric, Geophysical and Astronomical Services Administration (PAGASA). IDF relationships are usually in a graphical form with duration plotted on the horizontal axis, intensity on the vertical axis and a series of curves for each design return period (Chow et al., 1988). The design storms with a 10-minute interval were generated using this information. The hyetographs of the selected design storm were produced using the alternating block method which consist of incremental precipitation depth blocks placed on the time axis to generate the greatest precipitation depth for all durations shorter than the storm duration (Olivera et al., 2002).

In Figure 4.21, a simplified flowchart for running different flood scenarios is given. Five simulations were run in openLISEM in order to answer the related research questions. These scenarios are based on different LULC maps (1989 and 2016) and three design storms.

Scenario 1: Flood simulation using 1989 LULC map and rainfall data of Typhoon Ketsana (2009)
Scenario 2: Flood simulation using 2016 LULC map and rainfall data of Typhoon Ketsana (2009)
Scenario 3: Flood simulation using 2016 LULC map and rainfall data of 5YR- return period design storm
Scenario 4: Flood simulation using 2016 LULC map and rainfall data of 10YR- return period design storm
Scenario 5: Flood simulation using 2016 LULC map and rainfall data of 20YR- return period design storm

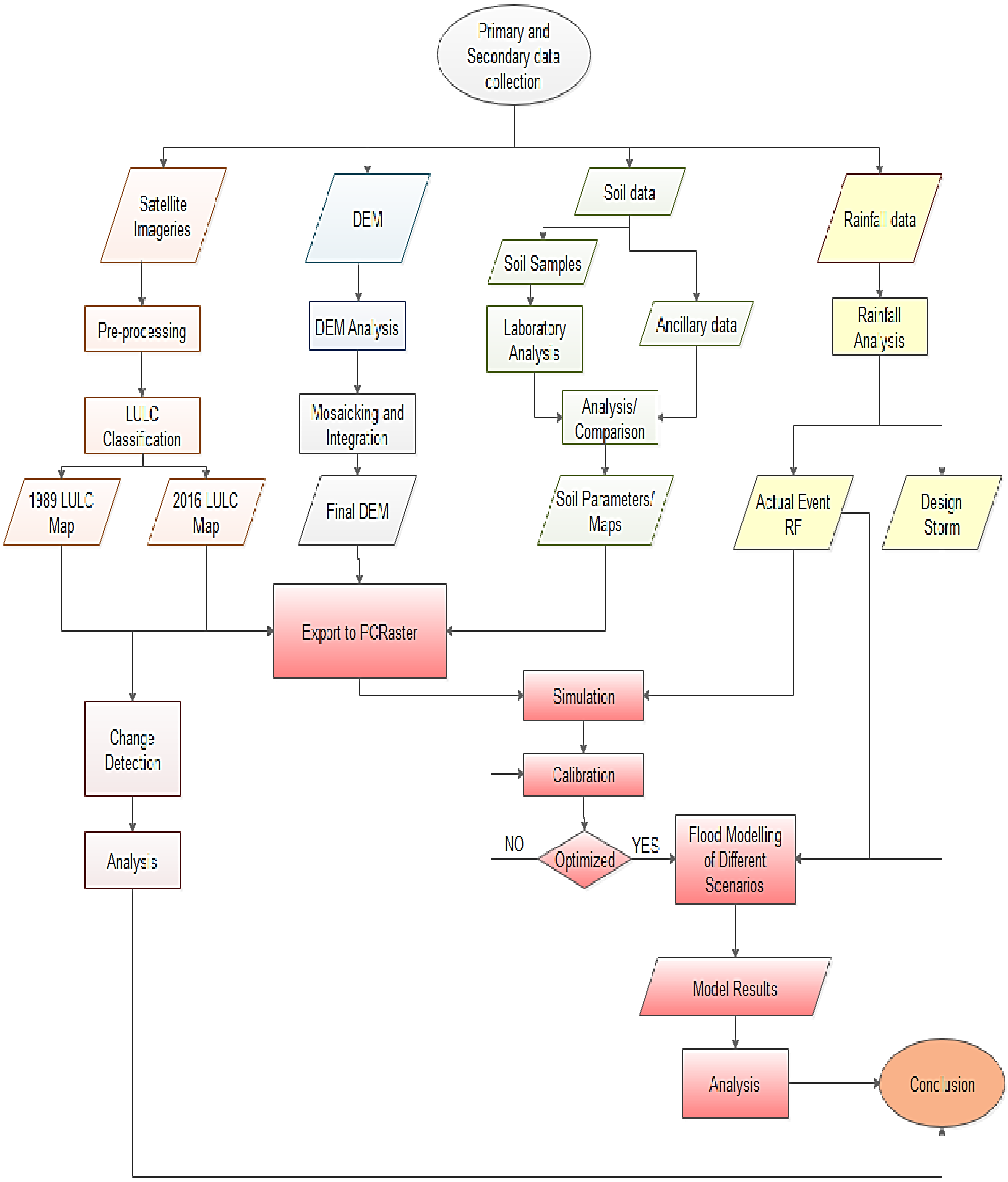

Figure 4.21 Flow chart showing the simplified methodology of the research work

5. RESULTS AND DISCUSSION

5.1. Land use and land cover Classification

For the LULC classification of 1989 and 2016 Landsat images (Figure 5.1) using spectral angle mapper (SAM) algorithm, six (6) general categories of land cover were distinguished based on a-priori knowledge of the area and previous studies which include forest, shrub, grass, agriculture, built-up and water body (Abino et al., 2015) (Figure 5.2). Classified maps show that grassland was the dominant land cover type in both years. In 1989, forest was the second extensive land cover followed by shrub, built-up, agriculture and water body as the least. However, in 2016, forest was replaced by built-up and shrub while agriculture and water body are the least land cover type (Table 5.1).

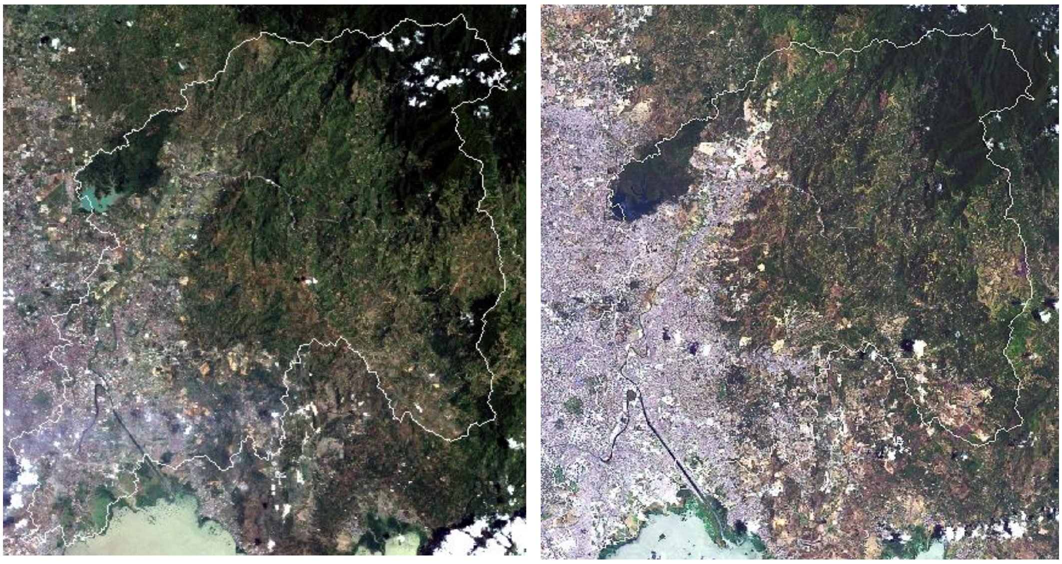

Figure 5.1 (Left) Landsat TM 7 satellite image of the study area in 1989; (Right) Landsat OLI-8 image of MRB in 2016

Table 5-1 Total Area coverage of various land cover types

LULC Class	1989	2016
	Area (hectares)	
Forest	18, 683	13,350
Shrub	14,470	13,197
Grass	20,841	21,640
Agriculture	2,850	3,832
Built-up	11,928	16,952
Water Body	821	622

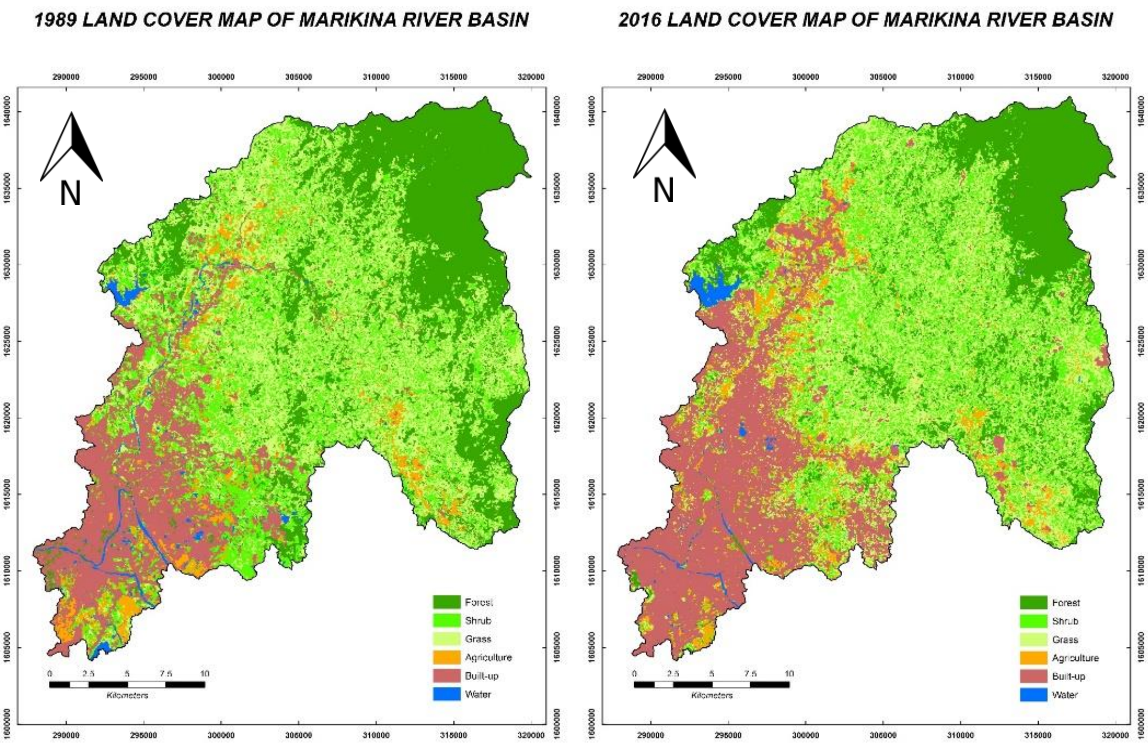

Figure 5.2 Land cover map of MRB in 1989 and 2016 generated from Landsat imageries

Tables 5.2 presents the producer's and user's accuracy statistics and error matrix, respectively of 1989 image while tables 5.3 shows the results for 2016 image. Result of the accuracy assessment using 40 test pixels for 1989 shows an overall accuracy of 70% was reached with an overall Kappa (K^) statistics of 0.6404. For 2016, 48 test pixels were used and yielded an overall accuracy of 77.08% and K^ statistics of 0.7202.

Table 5-2 Error Matrix and accuracy report for 1989 classified image

Land Cover	***Forest***	***Shrub***	***Grass***	***Agriculture***	***Built-up***	***Water body***	***Classified Totals***	***Reference Totals***	***Number Correct***	***Producers Accuracy***	***Users Accuracy***
Forest	6	4	0	0	1	0	11	7	6	85.71%	54.55%
Shrub	1	1	2	0	0	0	4	8	1	12.50%	25.00%
Grass	0	3	3	0	0	0	6	5	3	60.00%	50.00%
Agriculture	0	0	0	6	0	0	6	7	6	85.71%	100.00%
Built-up	0	0	0	0	6	0	6	7	6	85.71%	100.00%
Water Body	0	0	0	1	0	6	7	6	6	100.00%	85.71%
Totals	7	8	5	7	7	6	40	40	28		
								Overall Classification Accuracy			**70.00%**

Table 5-3 Error Matrix and accuracy report for 2016 classified image

Land Cover	***Forest***	***Shrub***	***Grass***	***Agriculture***	***Built-up***	***Water body***	***Classified Totals***	***Reference Totals***	***Number Correct***	***Producers Accuracy***	***Users Accuracy***
Forest	10	0	0	0	0	0	10	13	10	76.92%	100.00%
Shrub	1	6	1	1	0	0	9	8	6	75.00%	66.67%
Grass	1	1	6	1	0	0	9	9	6	66.67%	66.67%
Agriculture	1	1	1	4	0	0	7	6	4	66.67%	57.14%
Built-up	0	0	1	0	8	1	10	8	8	100.00 %	80.00%
Water Body	0	0	0	0	0	3	3	4	3	75.00%	100.00%
Totals	13	8	9	6	8	4	48	48	37		
								Overall Classification Accuracy			**77.08%**

Based on the matrices, it shows that in general, the classification accuracy of shrub and grass is relatively low. This could be explained due to overlapping occurrence of these land covers. On the field, grass and shrub occur as intergrowth in very close range, thus, labelling of entire 30-m pixel to one category will result to some error. Moreover, the insufficiency of test samples per category may also be a limitation as not all spectral signatures of each category could have been represented.

5.2. Land cover change detection

The independently generated LULC maps were then subjected to change detection analysis in ERDAS Imagine using post classification method specifically matrix union and summary report of matrix function as described in section 4.1.2. The former produced an output image file which shows how classes between the two images overlap. The summary report produced a cross-tabulation statistics between the two thematic image file which shows a "from-to" change of classes in either number of points, area or percentage.

The summary matrix of the post classification method displays the change of land cover based land area in hectare (Table 5.4) wherein each column for every land cover type totals to the area covered in 1989, while the rows show the area of change from one class to another.

Based on the analysis, the highest general change (excluding water body) was on the agricultural land wherein of its original 2,849 hectares in 1989, about 2,156 hectares was converted into a different land cover. The largest conversion of agricultural land was into built-up area which accounts to a sizeable portion of 1195.47 hectares. This may be attributed to the high demand and value of land for residential projects like subdivisions and condominiums as well as commercial buildings. Forest and shrubs were mainly changed to grassland that may be due to some slash and burn practices ("kaingin") or clearing.

Comparison of gain and loss reveals that forest cover has the largest loss in terms of area from 1989 to 2016 of about 5,333 hectares, followed by shrub with 1,272 hectares loss. Built-up on the other hand, gained an additional area of about 5,023 hectares followed by agriculture and grass which gained 982 hectares and 798 hectares, respectively. However, it should be noted that the result also produced some questionable results which can be attributed to classification accuracy.

Table 5-4 Summary matrix showing area of land cover change from 1989 to 2016 using post classification method

		1989							
		Area (Hectares)							
Land Cover Type		Forest	Shrub	Grass	Agriculture	Built-up	Water Body	***GAIN***	***Total Area***
2016	Forest	9820.89	513.63	2843.01	68.67	58.32	45.45	*3529.08*	**13349.97**
	Shrub	3178.98	7133.04	2139.84	336.69	373.14	35.73	*6064.38*	**13197.42**
	Grass	4836.69	3268.89	12158.82	525.96	784.44	64.98	*9480.96*	**21639.78**
	Agriculture	193.32	877.86	1335.96	692.82	621.18	110.61	*3138.93*	**3831.75**
	Built-up	627.93	2593.26	2257.2	1195.47	9998.28	280.17	*6954.03*	**16952.31**
	Water Body	25.29	83.52	106.65	30.15	92.97	283.77	*338.58*	**622.35**
	Total Area	**18683.1**	**14470.2**	**20841.48**	**2849.76**	**11928.33**	**820.71**		
	LOSS	*8862.21*	*7337.16*	*8682.66*	*2156.94*	*1930.05*	*536.94*		

Visual inspection and comparison between 1989 LULC map and 2016 LULC map shows that there is a significant increase of built-up areas north-eastward (Figure 5.3a). Analysis of the socioeconomic status within the watershed reveals that increase of population growth rate can also be observed in the similar areas. Expansion of land development particularly subdivisions is attributed to the increasing population and high market value which is also likely related to industrialization. According to the Formulation of an Integrated River Basin Management and Development Master Plan for Marikina River Basin, industrial land and commercial areas have been rapidly developing in the past 10 years.

Moreover, there was also a considerable decrease of forest cover from 18,683 hectares in 1989 to 13,350 hectares in 2016 (Figure 5.4a). As per DENR report (IRBMP, 2015), small-scale charcoal making and "kaingin" contributed to the degradation and deforestation of the upper reaches of the catchment. Change analysis shows that large portion of the forest cover in 1989 became shrub and grassland while areas at the lower catchment has been converted to built-up area which increase (Figure 5.4b).

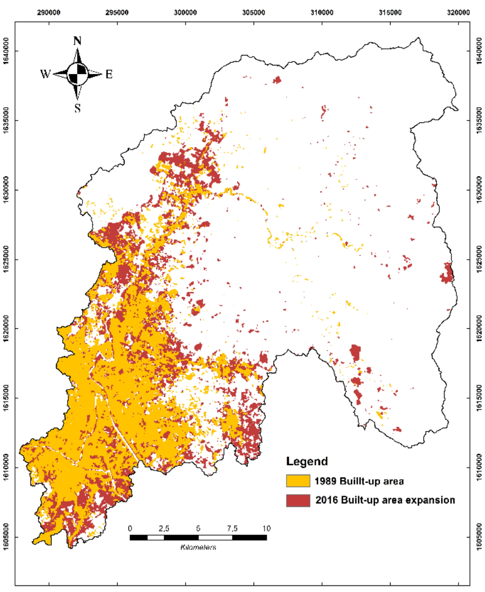

Figure 5.3 Spatial distribution of built up areas within the last 3 decades

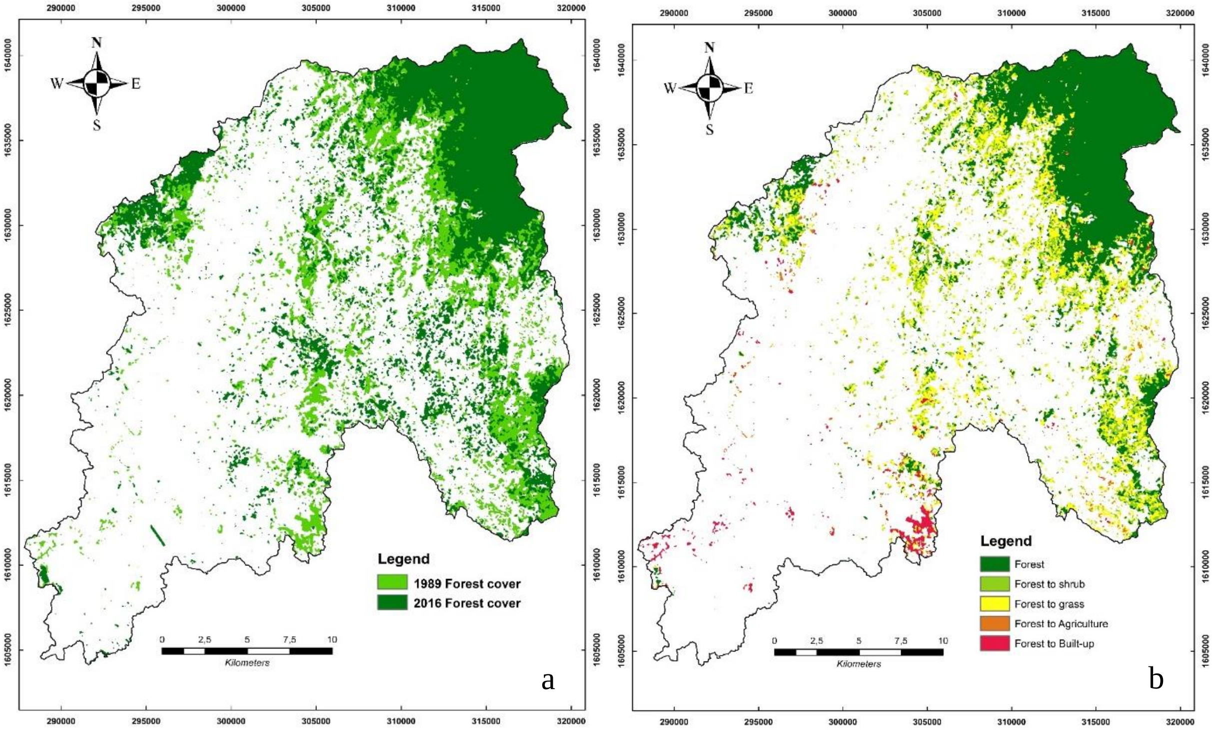

Figure 5.4 (a) significant decrease of forest cover from 1989 to 2016 shown spatially; (b) conversion from forest cover to other land covers

5.3. Rainfall-runoff modelling and calibration

Rainfall-runoff and flashflood simulation was carried out using the actual extreme rainfall of Typhoon Ketsana in 2009. The model generates a hydrograph which shows rainfall and discharge against time as well as information on channel water height. The result of the model was compared to a set of measured values of water level from Sto. Niño gauging station for calibration. Calibration is done in order to achieve an acceptable level of predictive quality and optimize the parameter setting (ITC Core Book, 2012). In this research, optimization of parameters was performed by fine tuning the Ksat values and Manning's n of both slopes and channel. These parameters both influence the infiltration rate, surface runoff generation and response time of discharge.

The measured water level in Sto. Niño gauging station included the base flow height within the channel, as such, the values were subtracted with the assumed base flow level prior to the flooding event which is 15.8 meters. Moreover, the measured water level values considered in the calibration only covered the time period from 0500H (900 min) to 1800H (1680 min) as no measurement was available after the last record.

However, due to time constraints, calibration done by trial and error method was limited by generating a hydrograph with a closest fit to the observed water level which in this case was obtained by using a multiplication factor of 2.0 for both Manning's n and Ksat (Figure 5.5).

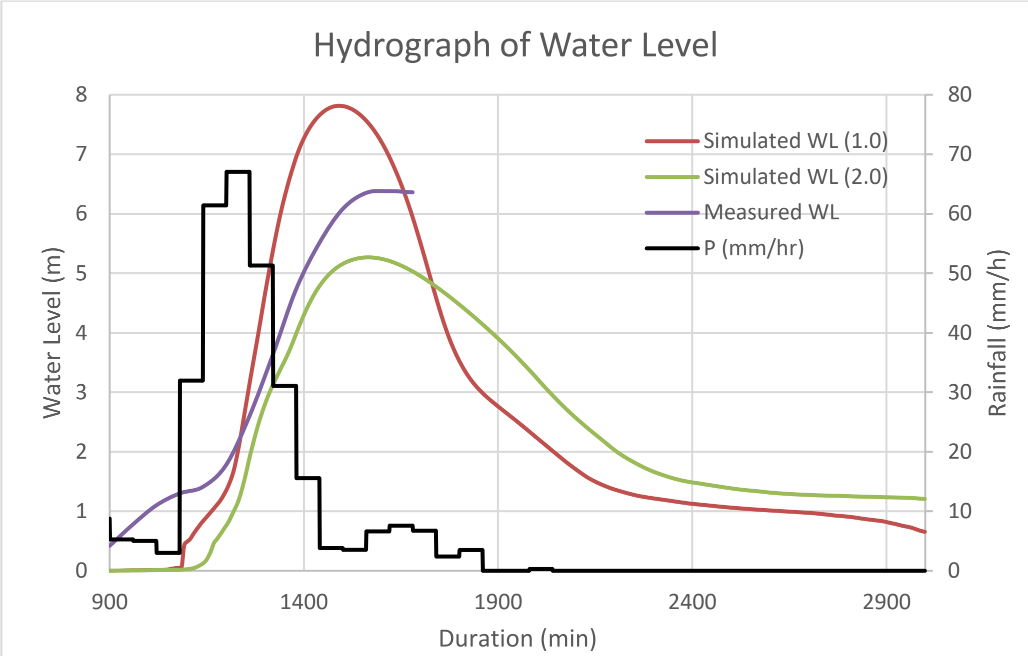

Figure 5.5 OpenLISEM calibration result showing the nearest simulated curve (green) to the measured water level value at Sto. Niño Gauging station

5.4. Impact of Land use/ Land cover

In this research, the impact of LULC change on runoff generation was assessed by simulating flood scenarios using similar rainfall data to different LULC map from two periods. Earlier analysis of satellite images verified the significant changes in land cover from 1989 to 2016 particularly at the upper reaches of the watershed from forest to shrub/grass while change from agriculture to built-up was noted within the floodplain of the catchment.

As illustrated in section 4.3.1, decrease in vegetation cover is in accord with the increase of built up area. The reduction of cover is associated to the decrease in leaf area index (LAI) (see Figure 4.16) which determines the interception storage capacity especially in the upper catchment (Figure 4.17). In the study of Siriwardena et al. (2006), they concluded that the impact of clearing forest vegetation in the Comet catchment in Central Queensland from 83% to 38% increase the runoff by about 40%. This was also established in the work of Lin & Wei (2008) where they correlated the decrease of forest to the significant increase in peak and mean flows

In this study, it can be noted that vegetation cover in 1989 is widespread as compared to 2016, thus, it is expected that run-off will also be low during this period due to high vegetation interception. To assess whether this concept holds true to my study area, it is necessary to quantify the effect of land cover change particularly upstream which is considered as the run-off originating zone (Wang et al., 2006b). In doing so, outpoint 1 (refer to Figure 4.20) was used to record the simulated peak time and peak discharge of scenarios 1 and 2 as described in section 4.3.2.

When the rainfall-runoff model was run using the 27 hour rainfall duration with an average total rainfall of about 300mm on the land cover map of 1989, the peak discharge was **18m³/s** with peak time at **1328** minutes. Using the same rain event on 2016 land cover map, the peak discharge generated was **16m³/s** with peak time at 1211 minutes (Figure 5.6).

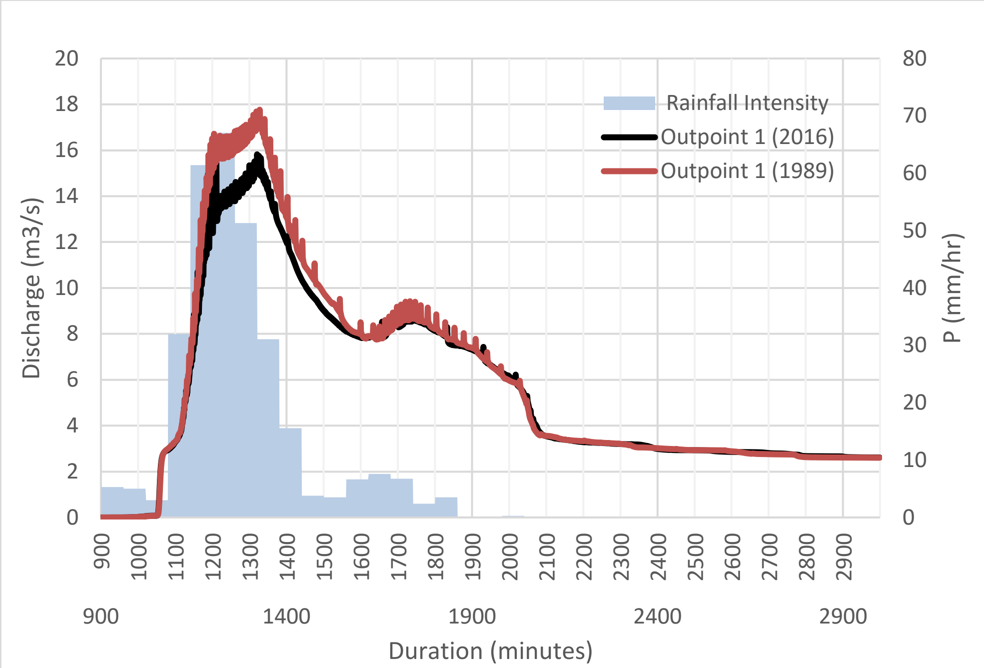

Figure 5.6 Hydrograph of the simulated discharge against rainfall between two years as measured in outpoint 1

Result shows that the decrease of forest cover in 2016 resulted to a slight decrease of runoff and discharge. This confirms the result of the work of Sriwongsitanon & Taesombat (2011) in which they stated that during high rainfall intensity events, watershed condition behaves differently especially in catchments with high antecedent soil moisture. Based on their research, forest area can have high antecedent soil moisture from previous rain events due to deeper root zone and higher soil moisture holding capacity and will entail less amount of water to reach saturation stage thus resulting to higher runoff. They concluded that an increase in forest area also increased the runoff coefficient and increase in non-forest area resulted to lower runoff coefficient. This is characterized by the total discharge (Q_{total}) produced by the model for both dataset, where Q_{total} **= 9.4 million m³** and **7.6 million m³** for 1989 and 2016, respectively.

For the downstream part of the catchment, the significant LULC change was the increase of built up areas from 17% of the total area in 1989 to 24% 2016. Urbanization in the floodplain adversely influence the hydrological processes in the lower catchment by decreasing the infiltration capacity of the underlying soil attributed to the increase of impervious surfaces. This will result to higher runoff thus enhancing flood volume and extent. Model output shows that the peak discharge and peak time measured in outpoint 2 (refer to figure 4.20) on 1989 LULC map was 103 m³/s at 1561 minutes while on 2016 LULC was 116 m³/s at 1566 minutes (Figure 5.7). Flood volume and flooded area in 1989 is **84.3 million m³** and **103.4 million m²,** respectively, while for 2016 is **86 million m³** and **103.7 million m²**.

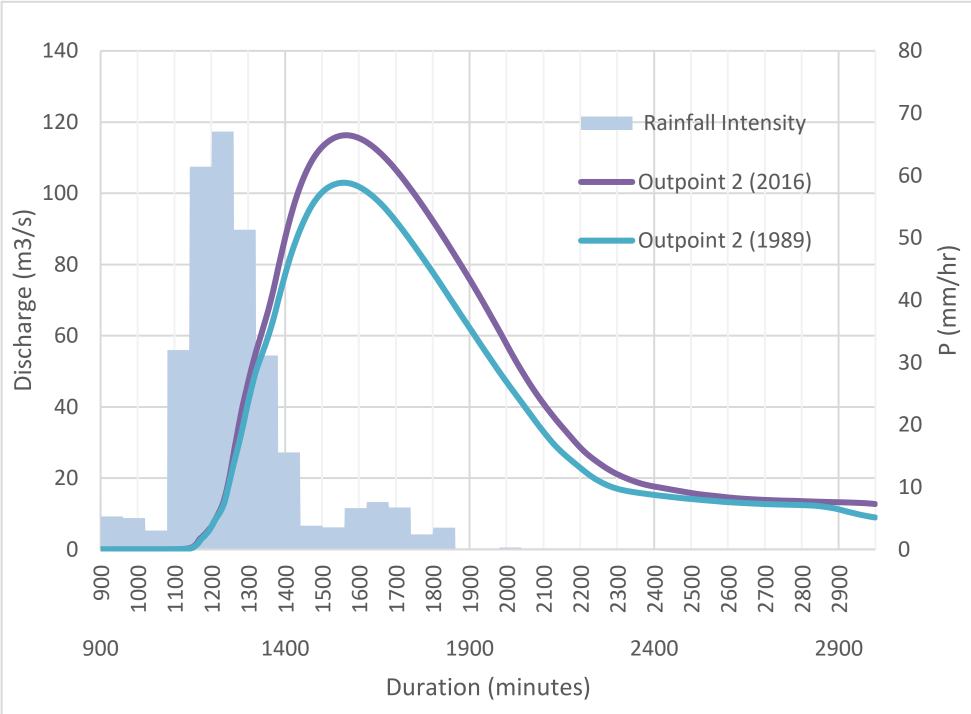

Figure 5.7 Hydrograph of the simulated discharge against rainfall between two years as measured in outpoint 2

Moreover, another consequence of reduced infiltration rate is longer flood duration for 2016 as shown in Figure 5.8. Duration difference of flood between the two scenarios is noticeable wherein a considerable area in 2016 experienced flood in a longer period as compared to 1989. This is attributable to expansion of built-up areas wherein the increase of hard surfaces greatly reduced the infiltration rate within the floodplain. Moreover, intensification of construction may have also lead to the increase of obstruction to surface runoff thus limiting the flow of water to natural or artificial channels increasing flooding period in the lowland.

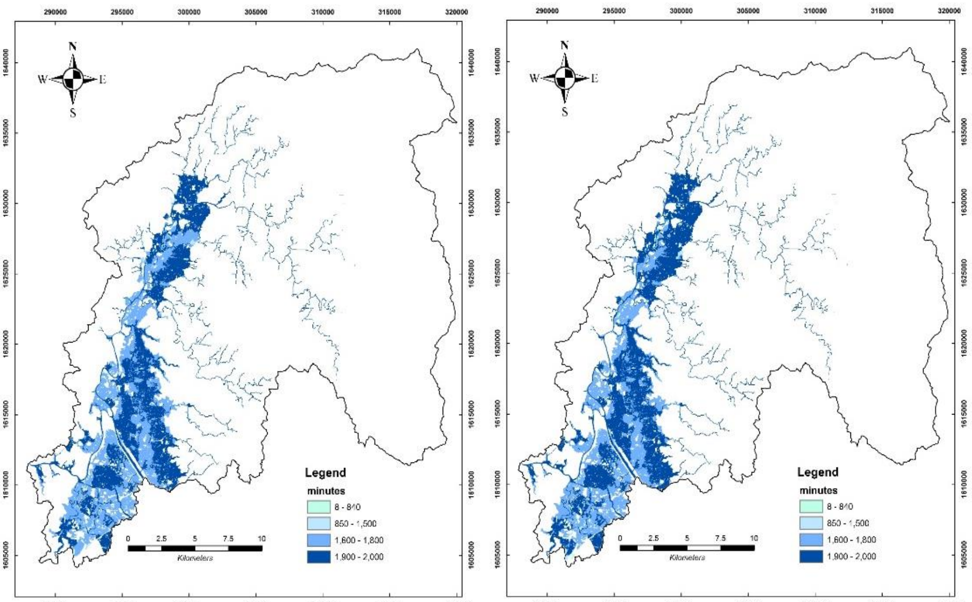

Figure 5.8 Flood duration map of 1989 (left) and 2016 (right)

The summary of simulation result is presented in Table 5-7. This shows that overall, LULC change has minimal impact on flooding occurrences during extreme condition.

Table 5-4 Results of OpenLISEM flood model

Variable	Unit	1989	2016
LISEM results at time	min	2,998	2,998
Catchment area	Ha	73,334.07	73,334.07
Total Precipitation	mm	306.3	306.3
Total discharge	mm	23.11	21.10
Total interception	mm	0.63	0.63
Total House interception	mm	0.10	0.15
Total infiltration	mm	146.17	142.41
Surface storage	mm	0.02	0.02
Water in runoff + channel	mm	22.42	20.93
Total discharge	m^3	9.4×10^6	7.6×10^6
Peak time precipitation	min	1,201	1,201
Peak discharge/Precipitation	%	7.54	6.89
Flood volume (max level)	m^3	84×10^6	86×10^6
Flood area (max level)	m^2	103.4×10^6	103.7×10^6

5.5. Response of large watershed to varying flood return period

To evaluate how a large watershed such as MRB responds to extreme rainfall at different return periods, 4-hour design rain storms at 10-minutes time steps for 5-yr, 10-yr and 20-yr return period were generated using IDF curves and alternating block method as illustrated in section 4.2.2. The total precipitation used for each return period are 138mm (5-yr RP), 169mm (10-yr RP) and 198mm (20-yr RP). Flood simulations for different return periods were undertaken using LULC map of 2016 in OpenLISEM. Two outlet points were considered in assessing hydrologic responses of the upper and lower watershed (Figure 5.9).

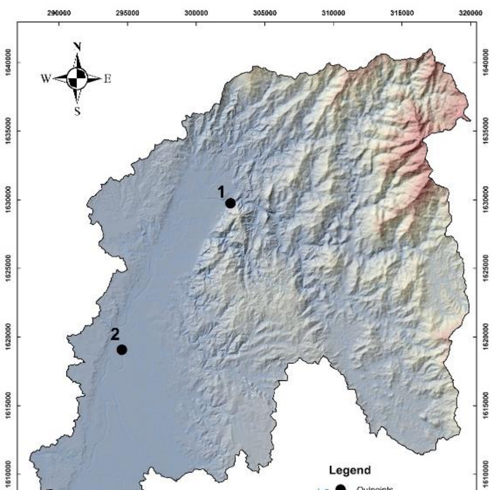

Figure 5.9 Outpoint locations

Result shows that in the upper catchment, the increase of return period only induced a minimal increase on peak discharge as measured from outpoint 1 (Table 5-6). The peak discharge is highest in the 20y-return period at 18 m^3/s while the lowest is recorded for the 5y-RP at 16 m^3/s (Figure 5.10). However, this also suggests that as rainfall intensity increases, effect of vegetative covers in terms of interception becomes negligible resulting to more water available for surface runoff.

Table 5-5 Discharge data at outpoint 1

	5y-RP	10y-RP	20y-RP
Peak discharge ($m^{3/s}$)	15.6	17.3	18.2
Peak time discharge (min)	141	143	148

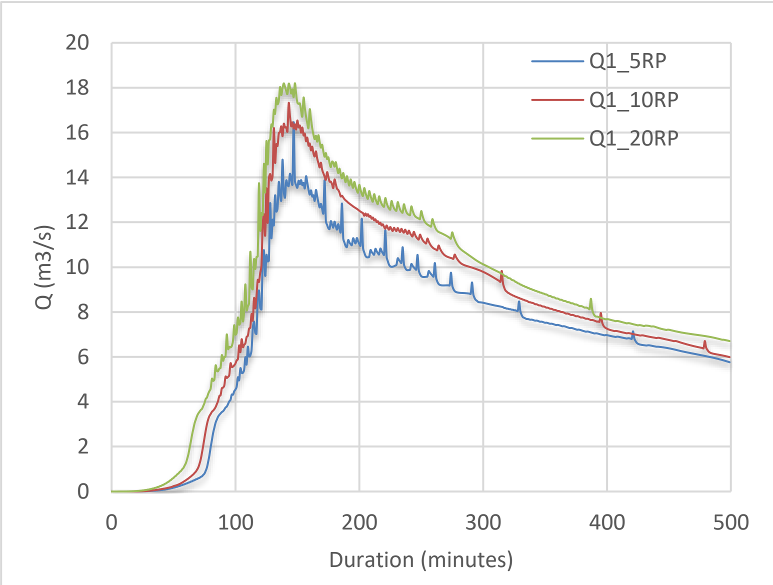

Figure 5.10 Hydrograph measured at outpoint 1

On the other hand, distinct variation on flood characteristics are more observable in the downstream area as measured at outpoint 2 (Table 5-6). A significant difference on peak discharge and peak timing was noted wherein increase in return period denotes high peak discharge and shorter response time (Figure 5.11). The peak discharge and peak timing for 5-, 10- and 20y-RP are 40 m^3/s at 498min, 57 m^3/s at 448 and 77 m^3/s at 426 min, respectively.

Table 5-6 Discharge data at outpoint 2

	5y-RP	10y-RP	20y-RP
Peak discharge ($m^{3/s}$)	40.36	56.88	77.08
Peak time discharge (min)	498	448	426

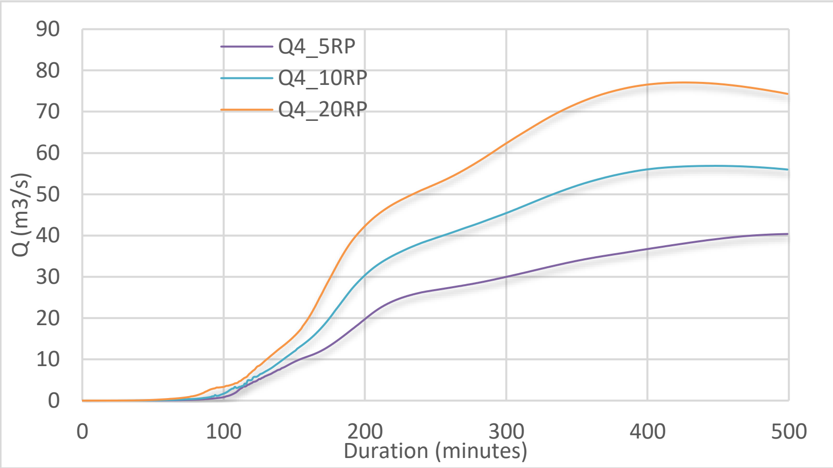

Figure 5.11 Hydrograph measured at outpoint 2

Table 5-7 displays the summary of the simulation run in OpenLisem for the 3 return period in terms of flood characteristics. Result clearly shows that an approximate 30mm difference of total precipitation will yield to a significant increase in flood characteristic. This changes are illustrated in Figure 5.12 wherein comparison of flood depth map clearly shows that with increasing return period, extent of areas inundated with higher water depth (> 2 meters) increases especially at the lower catchment. This may also be attributed to the runoff contribution of other smaller tributaries to the west which drains towards lowland area.

Table 5-7 Summary statistics of the flood simulation for the 3 return periods

	Unit	**5RP**	**10RP**	**20RP**
Total Precipitation	mm	137.85	169.1	198.25
Total discharge	mm	2.90	3.96	4.99
Total interception	mm	0.63	0.63	0.58
Water in runoff + channel	mm	18.44	28.44	25.05
Total discharge	m^3	7.9×10^5	10.1×10^5	12.8×10^5
Peak discharge/Precipitation	%	2.10	2.34	2.52
Flood volume (max level)	m^3	41×10^6	53×10^6	66×10^6
Flood area (max level)	m^2	86×10^6	94×10^6	99×10^6

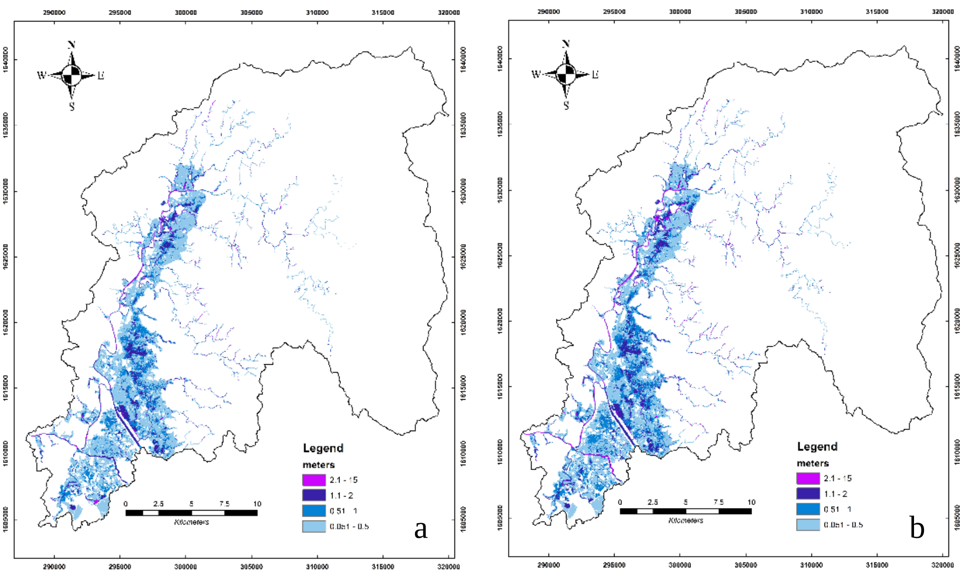

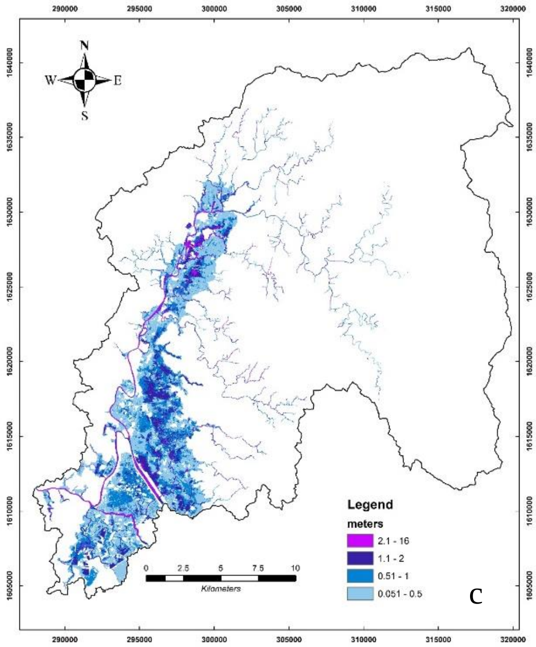

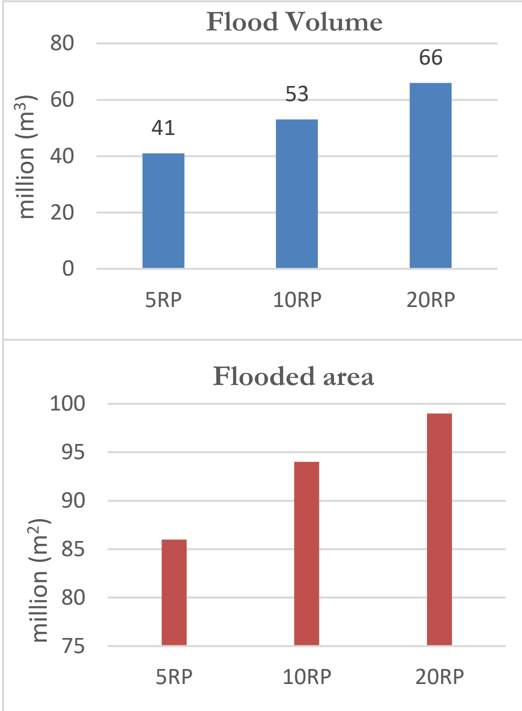

Figure 5.12 Flood depth and flood extent map of (a) 5yr-RP, (b) 10yr-RP and (c) 20yr-RP. Graphs on right illustrates the statistical differences of flood depth and flood extent for the 3 return periods

5.6. Validation of simulated result (2016 Scenario)

The simulated model for scenario 1 using rainfall data during typhoon Ketsana was validated by comparing the flood depth map with the published flood map of the Mines and Geosciences Bureau (MGB). MGB flood map is based worst case event in the area and mainly used flood depth and flood duration as parameters for classification (Appendix D). Comparison of simulated flood depth and flood extent with MGB flood susceptibility map is illustrated in Figure 5.13.

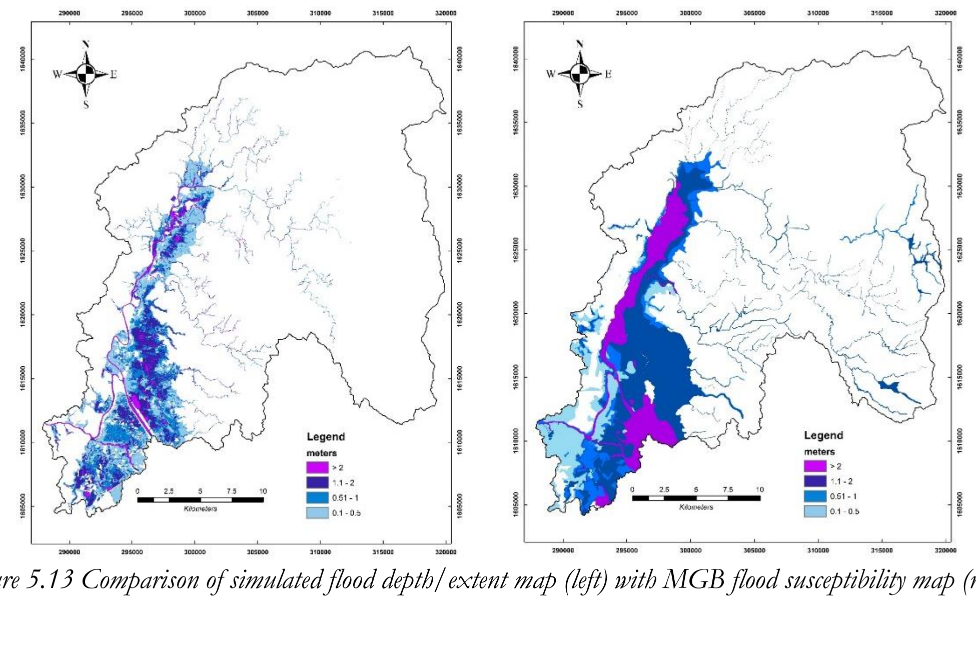

Figure 5.13 Comparison of simulated flood depth/extent map (left) with MGB flood susceptibility map (right)

Validation shows that the simulated result closely resembles the flood susceptibility map in terms of extent. In terms of flood depth, it can be noted that some portions of the model output have discrepancy as compared to the delineated zones of MGB. This however, still needs additional validation with flood depth measurement during the actual flooding event

5.7. Scope and Limitation of the Research

This research covers the MRB with a total area of 698 sq. km. Taking into account the size of the watershed, the study was limited to few free remotely sensed products to cover the whole area with a reasonable spatial resolution and high temporal resolution. In this case Landsat TM 5 and OLI-8 with 30-m spatial resolution were used for the land cover classification.

Moreover, the samples collected from field were not sufficient to represent the different soil types and landcover types of the area. Therefore, laboratory results of the falling head permeability test for hydraulic conductivity analysis and soil textural analysis using pipette method were only used for comparison and confirmation, respectively. Instead, published secondary data were utilized in the parameterization of the model.

Likewise, effect of structures within the floodplain particularly the Manggahan floodway and Napindan Channel were disregarded in the flood simulation using the extreme rainfall record during the onset of typhoon Ketsana (TS "Ondoy") in 2009. In reality, these two structures influence the discharge and flow velocity along the main river by diverting flood water to the nearby Laguna de Bay. This could have affected the total discharge as well as the flood extent and depth in the simulation.

Furthermore, due to time constraints and the period required in undertaking each simulation which is about 72 hours, calibration and validation of the model was limited. In this work, a multiplication factor of 2 for both Ksat and Manning's n was considered as the best option for the time being in running the model. This limitation may introduce some inaccuracies in the reported output of the simulation which will give a discrepancy from the measured values. More time would have been useful for more intensive model calibration.

6. CONCLUSION AND RECOMMENDATION

In this research work, a physically-based model – OpenLISEM – was used to simulate the runoff and flashflood scenarios. As part of the research objective, LULC change was identified between the selected period (1989 and 2016) to established significant changes within the area. Analysis shows that the most dominant changes observed are the decrease of forest cover into shrub and grass at the upper reaches of MRB and the increase of built-up areas at the lowland that compensated the decrease of agricultural area. In general, these changes are mainly attributed to several driving factors such as human drivers (population growth), economic conditions and local upland practices (slash and burn).

The OpenLISEM model was able to simulate flood scenarios using the classified LULC map of 1989 and 2016. The result of the study as discussed in previous chapters showed that land use land cover change may have an influence to flashflood, however, several factors should also be considered. Analysis of the upstream area concludes that change of vegetative cover will have an insignificant effect to runoff generation during convective or extreme conditions. In the downstream part, urbanization have an effect on flood extent, flood volume and flood duration.

Moreover, simulation of scenarios using design storm of 5y-, 10-y and 20-y return period revealed that increase of rainfall intensity diminishes the influence of vegetative land covers to flood characteristics. In the contrary, development of infrastructures within the floodplain may impact the routing of runoff which may ensue changes to other flood properties such as depth, extent and duration.

In conclusion, the work undertaken was able to meet the research objectives in detecting significant land cover/land use change in MRB and in evaluating the influence of various LULC change to overland flow with extreme rains of different return periods. However, results of the study and performance of the model can be further improved if the following are taking into account:

- Produce a more accurate LULC maps by imploring other classification algorithms. Additional images from other periods can also be considered in order to establish a more concrete relationship between LULC change and runoff-flash flood.
- Determine physical soil properties such as saturated hydraulic conductivity of each land use/landcover per soil type to generate a more accurate representation of the study area
- Proper calibration and validation of model output is necessary to be able to generate a more realistic simulation. Acquisition of a complete data for calibration and validation is also needed
- Taking into account the required simulation time needed for this research, improvement to the model's algorithm or system can be look into in order to optimize the applicability of the model for large-scale watershed.

LIST OF REFERENCES

Abino, A. C., Kim, S. Y., Jang, M. N., Lee, Y. J., & Chung, J. S. (2015). Assessing land use and land cover of the Marikina sub-watershed, Philippines. *Forest Science and Technology*, *11*(2), 65–75. http://doi.org/10.1080/21580103.2014.957353

Abon, C. C., David, C. P. C., & Pellejera, N. E. B. (2011). Reconstructing the Tropical Storm Ketsana flood event in Marikina River, Philippines. *Hydrology and Earth System Sciences*, *15*, 1283–1289. http://doi.org/10.5194/hess-15-1283-2011

Abon, C. C., Kneis, D., Crisologo, I., Bronstert, A., David, C. P. C., & Heistermann, M. (2016). Evaluating the potential of radar-based rainfall estimates for streamflow and flood simulations in the Philippines. *Geomatics, Natural Hazards and Risk*, *7*(4), 1390–1405. http://doi.org/10.1080/19475705.2015.1058862

Aich, V., Liersch, S., Vetter, T., Fournet, S., Andersson, J. C. M., Calmanti, S., … Paton, E. N. (2016). Flood projections within the Niger River Basin under future land use and climate change. *Science of The Total Environment*, *562*, 666–677. http://doi.org/10.1016/j.scitotenv.2016.04.021

Almeida, C. A. de, Coutinho, A. C., Esquerdo, J. C. D. M., Adami, M., Venturieri, A., Diniz, C. G., … Gomes, A. R. (2016). High spatial resolution land use and land cover mapping of the Brazilian Legal Amazon in 2008 using Landsat-5/TM and MODIS data. *Acta Amazonica*, *46*(3), 291–302. http://doi.org/10.1590/1809-4392201505504

Archer, N. A. L., Bonell, M., Coles, N., MacDonald, A. M., Auton, C. A., & Stevenson, R. (2013). Soil characteristics and landcover relationships on soil hydraulic conductivity at a hillslope scale: A view towards local flood management. *Journal of Hydrology*, *497*, 208–222. http://doi.org/10.1016/j.jhydrol.2013.05.043

Badilla, R. A. (2008). *Flood Modelling in Pasig-Marikina River Basin.* (MSc Thesis), International Institute for Geo-Information Science and Earth Observation.

Baker, T. J., & Miller, S. N. (2013). Using the Soil and Water Assessment Tool (SWAT) to assess land use impact on water resources in an East African watershed. *Journal of Hydrology*, *486*, 100–111. http://doi.org/10.1016/j.jhydrol.2013.01.041

BBC News. (2014). Retrieved from http://news.bbc.co.uk/2/hi/europe/4913182.stm

Beven, K. J., Wood, E. F., & Sivapalan, M. (1988). On hydrological heterogeneity --Catchment Morphology and Catchment Response. *Journal of Hydrology Elsevier Science Publishers B.V*, *100*, 353–375.

Bi, Y., Zou, H., & Zhu, C. (2014). Dynamic monitoring of soil bulk density and infiltration rate during coal mining in sandy land with different vegetation. *International Journal of Coal Science & Technology*, *1*(2), 198–206. http://doi.org/10.1007/s40789-014-0025-2

Carating, R. B., Galanta, R. G., & Bacatio, C. D. (2012). *The Soils of the Philippines*. (A. Hartemink, Ed.)*National Science* …. Dordrecht: Springer London. http://doi.org/10.1007/978-94-017-8682-9

Chappell, N., Stobbs, A., Ternan, L., & Williams, A. (1996). Localised impact of Sitka spruce (Picea sitchensis (Bong.) Carr.) on soil permeability. *Plant and Soil*, *182*, 157–169.

Chow. (1959). Manning's n Values. Retrieved from http://www.fsl.orst.edu/geowater/FX3/help/8_Hydraulic_Reference/Mannings_n_Tables.htm

Chow, V. T., Maidment, D. R., & Mays, L. W. (1988). *Applied Hydrology*. (B. J. . Clark & J. Morriss, Eds.) (Internatio). Singapore: McGraw-Hill Book Co.

Coppin, P., Jonckheere, I., Nackaerts, K., Muys, B., & Lambin, E. (2004). *Digital change detection methods in ecosystem monitoring: a review. International Journal of Remote Sensing* (Vol. 25). Retrieved from http://www.tandfonline.com/doi/abs/10.1080/0143116031000101675

Costa, M. H., Botta, A., & Cardille, J. A. (2003). Effects of large-scale changes in land cover on the discharge of the Tocantins River, Southeastern Amazonia. *Journal of Hydrology*, *283*(1), 206–217. http://doi.org/10.1016/S0022-1694(03)00267-1

de Barros, C. A. P., Minella, J. P. G., Dalbianco, L., & Ramon, R. (2014). Description of hydrological and erosion processes determined by applying the LISEM model in a rural catchment in southern Brazil. *Journal of Soils and Sediments*, *14*(7), 1298–1310. http://doi.org/10.1007/s11368-014-0903-7

De Roo, A.P.J, Offermans, R. J. E, Cremers, N. H. D. . (1996). LISEM: A single-event, physically based hydrological and soil erosion model for drainage basins. II: Sensitivity analysis, validation and

application. *Hydrological Processes*, *10*(8), 11 19-1126. http://doi.org/10.1002/(SICI)1099-1085(199608)10:8<1119::AID-HYP416>3.0.CO;2-V
De Roo, A. P. J., Wesseling, C. G., & Ritsema, C. J. (1996). Lisem: A Single-Event Physically Based Hydrological and Soil Erosion Model for Drainage Basins. I: Theory, Input and Output. *Hydrological Processes*, *10*(8), 1107–1117. http://doi.org/10.1002/(SICI)1099-1085(199608)10:8<1107::AID-HYP415>3.0.CO;2-4
Devi, G. K., Ganasri, B. P., & Dwarakish, G. S. (2015). A Review on Hydrological Models. *Aquatic Procedia*, *4*, 1001–1007. http://doi.org/10.1016/j.aqpro.2015.02.126
Dimitriou, E. (2011). Overland Flow (pp. 536–536). Springer Netherlands. http://doi.org/10.1007/978-90-481-3585-1_104
Dudley, D. M., Tate, K. W., Mcdougald, N. K., & George, M. R. (2002). *Factors Influencing Soil-Surface Bulk Density on Oak Savanna Rangeland in the Southern Sierra Nevada Foothills 1*.
Dunne, T. (1983). RELATION OF FIELD STUDIES AND MODELING IN THE PREDICTION OF STORM RUNOFF. *Journal of Hydrology Elsevier Science Publishers B.V*, *65*, 25–48.
Džubáková, K. (2010). Rainfall-Runoff Modelling: Its development, classification and possible applications. *ACTA GEOGRAPHICA UNIVERSITATIS COMENIANAE*, *54*(2), 173–181.
Elsenbeer, H. (2001). Hydrologic flowpaths in tropical rainforest soilscapes?a review. *Hydrological Processes*, *15*(10), 1751–1759. http://doi.org/10.1002/hyp.237
Food and Agriculture Organization of the United Nations. (2016). *GIEWS Update: Southeast Asia Flood Situation*.
Fujimoto, M., Ohte, N., & Tani, M. (2011). Effects of hillslope topography on runoff response in a small catchment in the Fudoji Experimental Watershed, central Japan. *Hydrological Processes*, *25*(12), 1874–1886. http://doi.org/10.1002/hyp.7943
Gale, Emma L.; Saunders, M. A. (2013). The 2011 Thailand flood: climate causes and return periods. *Weather*, *68*(9), 233–237. http://doi.org/10.1002/wea.2133
Global Assessment Report on Disaster Risk Reduction 2015. (n.d.). Retrieved May 31, 2016, from http://www.preventionweb.net/english/hyogo/gar/2015/en/home/data.php?iso=PHL
Haghnazari, F., Shahgholi, H., & Feizi, M. (2015). Factors affecting the infiltration of agricultural soils: review. *International Journal of Agronomy and Agricultural Research*.
Hillel, D. (1998). *Environmental Soil Physics*. *Academic Press San Diego CA*. http://doi.org/10.2134/jeq1999.00472425002800060046x
Horton, R. E. (1940). An approach toward a physical interpretation of infiltration capacity. In *Proceedings of Soil Science Society of America* (pp. 399–417).
Horton, R. E. (1945). Erosional development of streams and their drainage basins; hydrophysical approach to quantitative morphology. *BULLETIN OF THE GEOLOGICAL SOCIETY OF AMERICA*, *56*(40), 275–370.
Hu, J., & Zhang, Y. (2013). Seasonal Change of Land-Use/Land-Cover (LULC) Detection Using MODIS Data in Rapid Urbanization Regions: A Case Study of the Pearl River Delta Region (China). *IEEE Journal of Selected Topics in Applied Earth Observations and Remote Sensing*, *6*(4), 1913–1920. http://doi.org/10.1109/JSTARS.2012.2228469
Ilsever, M., & Unsalan, C. (2012). *Two-dimensional change detection methods: Remote sensing application*. Istanbul, Turkey: Springer. http://doi.org/10.1007/978-1-4471-4255-3
Jetten, V. (2002). LISEM Limburg Soil Erosion Model Windows version2.x Users Manual.
Kirkby, M. (1988). Hillslope runoff processes and models. *Journal of Hydrology Elsevier Science Publishers B.V*, *100*, 315–339.
Knebl, M. R., Yang, Z.-L., Hutchison, K., & Maidment, D. R. (2005). Regional scale flood modeling using NEXRAD rainfall, GIS, and HEC-HMS/RAS: a case study for the San Antonio River Basin Summer 2002 storm event. *Journal of Environmental Management*, *75*(4), 325–336. http://doi.org/10.1016/j.jenvman.2004.11.024
Knijff, J. Van der, Jones, R., & Montanarella, L. (1999). Soil erosion risk assessment in Italy. *Luxembourg: Office for Official Publications of the European Communities*, *EUR 19022*, 58. Retrieved from http://scholar.google.com/scholar?hl=en&btnG=Search&q=intitle:Soil+Erosion+Risk+Assessment+in+Italy#0
Kruse, F. a. (1994). Imaging spectrometer data analysis. *A Tutorial*, 12.
Kværnø, S. H., & Stolte, J. (2012). Effects of soil physical data sources on discharge and soil loss simulated

by the LISEM model. *CATENA*, *97*, 137–149. http://doi.org/10.1016/j.catena.2012.05.001
Li, C., Wang, J., Wang, L., Hu, L., & Gong, P. (2014). Comparison of Classification Algorithms and Training Sample Sizes in Urban Land Classification with Landsat Thematic Mapper Imagery. *Remote Sensing*, *6*(2), 964–983. http://doi.org/10.3390/rs6020964
Lin, Y., & Wei, X. (2008). The impact of large-scale forest harvesting on hydrology in the Willow watershed of Central British Columbia. *Journal of Hydrology*, *359*(1–2). http://doi.org/10.1016/j.jhydrol.2008.06.023
Liu, Q. ., Chen, L., Li, J. ., & Singh, V. . (2004). Two-dimensional kinematic wave model of overland-flow. *Journal of Hydrology*, *291*(1–2), 28–41. http://doi.org/10.1016/j.jhydrol.2003.12.023
Lu, D., Mausel, P., Brondízio, E., & Moran, E. (2004). Change detection techniques. *International Journal of Remote Sensing*, *25*(12), 2365–2401. http://doi.org/10.1080/0143116031000139863
Lu, D., & Weng, Q. (2007). A survey of image classification methods and techniques for improving classification performance. *International Journal of Remote Sensing*, *28*(5), 823–870. http://doi.org/10.1080/01431160600746456
Lunetta, R. S., & Elvidge, C. D. (Eds.). (1999). *Remote sensing cahnge detection: Environmental Monitoring methods and application*. London: Taylor and Francis Ltd.
Major River Basins in the Philippines. (n.d.). Retrieved August 21, 2016, from http://www.pagasa.dost.gov.ph/index.php/floods/major-river-basins-in-the-philippines
Manakos, I., & Braun, M. (Eds.). (2014). *Land Use and Land Cover Mapping in Europe* (Vol. 18). Dordrecht: Springer Netherlands. http://doi.org/10.1007/978-94-007-7969-3
Mas, J.-F. (1999a). Monitoring land-cover changes: a com parison of change detection techniques*. *Int. J. Remote Sensing*, *20*(1), 139–152.
Mas, J.-F. (1999b). Monitoring land-cover changes: A comparison of change detection techniques. *International Journal of Remote Sensing*, *20*(1), 139–152. http://doi.org/10.1080/014311699213659
McGlynn, B. L., & McDonnell, J. J. (2003). Quantifying the relative contributions of riparian and hillslope zones to catchment runoff. *Water Resources Research*, *39*(11), n/a-n/a. http://doi.org/10.1029/2003WR002091
McGlynn, B. L., McDonnell, J. J., Seibert, J., & Kendall, C. (2004). Scale effects on headwater catchment runoff timing, flow sources, and groundwater-streamflow relations. *Water Resources Research*, *40*(7), n/a-n/a. http://doi.org/10.1029/2003WR002494
Moughal, T. A. (2013). Hyperspectral image classification using Support Vector Machine. *Journal of Physics: Conference Series*, *439*, 12042. http://doi.org/10.1088/1742-6596/439/1/012042
Natural Disaster Association. (n.d.). Retrieved from http://www.n-d-a.org/
Olivera, F., Stolpa, D., Assistant, P. E., & Manager, P. E. (2002). Effect of the stoorm hyetograph duration and shape on the watershed response.
Penna, D., Tromp-Van Meerveld, H. J., Gobbi, A., Borga, M., & Dalla Fontana, G. (2011). The influence of soil moisture on threshold runoff generation processes in an alpine headwater catchment. *Hydrol. Earth Syst. Sci*, *15*, 689–702. http://doi.org/10.5194/hess-15-689-2011
Philippine Atmospheric, Geophysical and Astronomical Services Administration. (n.d.). Retrieved August 11, 2016, from http://www.pagasa.dost.gov.ph/index.php/climate-of-the-philippines
Prawiranegara, M. (2014). ScienceDirect Spatial Multi-Criteria Analysis (SMCA) for Basin-Wide Flood Risk Assessment as a tool in improving spatial planning and urban resilience policy making: A case study of Marikina River Basin,Metro Manila -Philippines. *Procedia - Social and Behavioral Sciences*, *135*(135), 18–24. http://doi.org/10.1016/j.sbspro.2014.07.319
Raja, R. A. A., Anand, V., Kumar, A. S., Maithani, S., & Kumar, V. A. (2013). Wavelet Based Post Classification Change Detection Technique for Urban Growth Monitoring. *Journal of the Indian Society of Remote Sensing*, *41*(1), 35–43. http://doi.org/10.1007/s12524-011-0199-7
Ramesh, A. (2013). *Response of Flood Events to Land Use and Climate Change: Analyzed by Hydrological and Statistical Modeling in Barcelonnette, France. Phd Thesis* (Springer Theses). Springer Netherlands, Dordrecht. Retrieved from https://ezproxy.utwente.nl:2096/abstract/9789400755277
Rawat, J. S., Biswas, V., & Kumar, M. (2013). Changes in land use/cover using geospatial techniques: A case study of Ramnagar town area, district Nainital, Uttarakhand, India. *The Egyptian Journal of Remote Sensing and Space Science*, *16*(1), 111–117. http://doi.org/10.1016/j.ejrs.2013.04.002
Rawls, W. J., Brakensiek, D. L., & Miller, N. (1983). Green-ampt Infiltration Parameters from Soils Data. *Journal of Hydraulic Engineering*, *109*(1), 62–70. http://doi.org/10.1061/(ASCE)0733-

9429(1983)109:1(62)
Saghafian, B., Farazjoo, H., Bozorgy, B., & Yazdandoost, F. (2008). Flood intensification due to changes in land use. *Water Resources Management*, *22*(8), 1051–1067. http://doi.org/10.1007/s11269-007-9210-z
Shafri, H. Z. M., Suhaili, A., & Mansor, S. (2007). The Performance of Maximum Likelihood, Spectral Angle Mapper, Neural Network and Decision Tree Classifiers in Hyperspectral Image Analysis. *Journal of Computer Science*, *3*(6), 419–423. http://doi.org/10.3844/jcssp.2007.419.423
Singh, A. (1989). Digital change detection techniques using remotely-sensed data. *International Journal of Remote Sensing*, *10*(6), 989–1003. http://doi.org/10.1080/01431168908903939
Siriwardena, L., Finlayson, B. L., & McMahon, T. A. (2006). The impact of land use change on catchment hydrology in large catchments: The Comet River, Central Queensland, Australia. *Journal of Hydrology*, *326*(1), 199–214. http://doi.org/10.1016/j.jhydrol.2005.10.030
Smits, P. C., Dellepiane, S. G., & Schowengerdt, R. A. (1999). Quality assessment of image classification algorithms for land-cover mapping: A review and a proposal for a cost-based approach. *International Journal of Remote Sensing*, *20*(8), 1461–1486. http://doi.org/10.1080/014311699212560
Sriwongsitanon, N., & Taesombat, W. (2011a). Effects of land cover on runoff coefficient. *Journal of Hydrology*, *410*(3–4), 226–238. http://doi.org/10.1016/j.jhydrol.2011.09.021
Sriwongsitanon, N., & Taesombat, W. (2011b). Effects of land cover on runoff coefficient. *Journal of Hydrology*, *410*(3–4), 226–238. http://doi.org/10.1016/j.jhydrol.2011.09.021
Steinbrich, A., Leistert, H., & Weiler, M. (2016). Model-based quantification of runoff generation processes at high spatial and temporal resolution. *Environmental Earth Sciences*, *75*(21), 1423. http://doi.org/10.1007/s12665-016-6234-9
Subyani, A. M., & Al-Amri, N. S. (2015). IDF curves and daily rainfall generation for Al-Madinah city, western Saudi Arabia. *Arabian Journal of Geosciences*, *8*(12), 11107–11119. http://doi.org/10.1007/s12517-015-1999-9
Suriya, S., & Mudgal, B. V. (2012). Impact of urbanization on flooding: The Thirusoolam sub watershed – A case study. *Journal of Hydrology*, *412*, 210–219. http://doi.org/10.1016/j.jhydrol.2011.05.008
Van Mullem, J. A. (1991). Runoff and Peak Discharges Using Green-Ampt Infiltration Model. *Journal of Hydraulic Engineering*, *117*(3), 354–370. http://doi.org/10.1061/(ASCE)0733-9429(1991)117:3(354)
Wahlstrom, Margareta ; Guha-Sapir, D. (2015). The Human Costs of Weather Related Disasters. *The United Nations Office for Diaster Risk Reduction*, 37. http://doi.org/10.1017/CBO9781107415324.004
Wang, G., Zhang, Y., Liu, G., & Chen, L. (2006a). Impact of land-use change on hydrological processes in the Maying River basin, China. *Science in China Series D: Earth Sciences*, *49*(10), 1098–1110. http://doi.org/10.1007/s11430-006-1098-6
Wang, G., Zhang, Y., Liu, G., & Chen, L. (2006b). Impact of land-use change on hydrological processes in the Maying River basin, China. *Science in China, Series D: Earth Sciences*, *49*(10), 1098–1110. http://doi.org/10.1007/s11430-006-1098-6
Wikipedia. (2017). List of Floods. Retrieved from https://en.wikipedia.org/wiki/List_of_floods
Wu, M., Wu, C., Huang, W., Niu, Z., Wang, C., Li, W., & Hao, P. (2016). An improved high spatial and temporal data fusion approach for combining Landsat and MODIS data to generate daily synthetic Landsat imagery. *Information Fusion*, *31*, 14–25. http://doi.org/10.1016/j.inffus.2015.12.005
Xu, C. (2002). *Hydrologic Models*. Uppsala: Uppsala University.
Zhang, L., Nan, Z., Yu, W., & Ge, Y. (2016). Hydrological Responses to Land-Use Change Scenarios under Constant and Changed Climatic Conditions. *Environmental Management*, *57*(2), 412–431. http://doi.org/10.1007/s00267-015-0620-z
Zope, P. E., Eldho, T. I., & Jothiprakash, V. (2016). Impacts of land use–land cover change and urbanization on flooding: A case study of Oshiwara River Basin in Mumbai, India. *CATENA*, *145*, 142–154. http://doi.org/10.1016/j.catena.2016.06.009
Zubair, A. O. (2006). *Change detection in land use and land cover using Remote Sensing Data and GIS (A case study of Ilorin and its environs in Kwara State Nigeria). MSc Thesis*. University of Ibadan.

APPENDIX

Appendix A: Annual maximum 24-H rainfall (1996-2015) measured from Science Garden Rain Gauge Station, Diliman, Quezon City

Year	Max 24	Year	Max 24 (Sort)	Rank	Left Prob	Right Prob	Return Period
1996	104.4	1996	104.4	1	0.047619	0.952381	1.05
1997	156.6	2005	104.6	2	0.095238	0.904762	1.105263
1998	137.2	2001	110.4	3	0.142857	0.857143	1.166667
1999	204.8	2010	122	4	0.190476	0.809524	1.235294
2000	267	2008	125.6	5	0.238095	0.761905	1.3125
2001	110.4	2015	135.5	6	0.285714	0.714286	1.4
2002	246.4	2004	135.6	7	0.333333	0.666667	1.5
2003	137.4	1998	137.2	8	0.380952	0.619048	1.615385
2004	135.6	2003	137.4	9	0.428571	0.571429	1.75
2005	104.6	2007	147	10	0.47619	0.52381	1.909091
2006	159.6	1997	156.6	11	0.52381	0.47619	2.1
2007	147	2006	159.6	12	0.571429	0.428571	2.333333
2008	125.6	1999	204.8	13	0.619048	0.380952	2.625
2009	455	2013	225.7	14	0.666667	0.333333	3
2010	122	2002	246.4	15	0.714286	0.285714	3.5
2011	250.9	2011	250.9	16	0.761905	0.238095	4.2
2012	391.4	2000	267	17	0.809524	0.190476	5.25
2013	225.7	2014	268	18	0.857143	0.142857	7
2014	268	2012	391.4	19	0.904762	0.095238	10.5
2015	135.5	2009	455	20	0.952381	0.047619	21

Source: Philippine Atmospheric, Geophysical and Astronomical Services Administration (PAGASA)

Appendix B: Particle Size Analysis Calculation

The basis of the calculations is the oven-dry sample weight after all treatments. It is obtained by the summation of all individual fractions:

Clay (<2 µm)	= (H * 50) – (Z * 50)	(wt. K)
Silt (2-20 µm)	= (G * 50) – (Z * 50) – K	(wt. L)
Silt (20-50 µm)	= (F * 50) – (Z * 50) – K - L	(wt M)
Sand (>50 µm)	= A + B + C + D + E	(wt N)
Sample weight	= K + L + M + N	*weight all in grams

Where:

A through E	= weight of individual sand fractions
F	= weight 20ml pipette aliquot of fraction <50 µm
G	= weight 20ml pipette aliquot of fraction <20 µm
H	= weight 20ml pipette aliquot of fraction <2 µm
Z	= weight 20ml pipette aliquot of blank

Proportional amounts of the fractions can be calculated by:

$$\% \text{ clay } (<2\ \mu m) = \frac{K}{\text{sample wt.}} * 100$$

$$\% \text{ silt } (2\text{ -}2\ \mu m) = \frac{L}{\text{sample wt.}} * 100$$

$$\% \text{ silt } (20\text{-}50\ \mu m) = \frac{M}{\text{sample wt.}} *100$$

$$\% \text{ sand } (1000\text{-}2000\ \mu m) = \frac{A}{\text{sample wt.}} *100$$

$$\% \text{ sand } (500\text{-}1000\ \mu m) = \frac{B}{\text{sample wt.}} *100$$

$$\% \text{ sand } (250\text{-}500\ \mu m) = \frac{C}{\text{sample wt.}} *100$$

$$\% \text{ sand } (100\text{-}250\ \mu m) = \frac{D}{\text{sample wt.}} *100$$

$$\% \text{ sand } (50\text{-}100\ \mu m) = \frac{E}{\text{sample wt.}} *100$$

Source: Particle Size Analysis, ITC, Geoscience Lab.

Appendix C: Required input database format for OpenLisem

Variable name	***Data/Map name***
Rainfall	Rainfall file
	Id.map
Catchment	Dem.map
	Grad.map
	Ldd.map
	Outlet.map
	Outpoint.map
Landuse	LULC.map
	Per.map
	Lai.map
	Ch.map
	Roadwidt.map
	Grasswid.map
	Smax.map
Surface	rr.map
	n.map
	Stonefrc.map
	Crustfrc.map
	Compfrc.map
	Hardsurf.map
Infiltration (1st layer Green & Ampt)	Ksat1.map
	Psi1.map
	Thetas1.map
	Thetai1.map
	Soildep1.map
Channels (Channel Properties)	Lddchan.map
	Chanwidt.map
	Chanside.map
	Changrad.map
	Chanman.map
	Chancoh.map
Channel Flood	Chandepth.map
	Barriers.map
	Chanmaxq.map
	Chanlevee.map
	Hmxinit.map
	Floodzone.map
Houses	Housecover.map

Source: LISEM Manual version 2.x – January 2, 2002

Appendix D: Parameters used by Mines and Geosciences Bureau for Flood Mapping

FLOOD SUSCEPTIBILITY PARAMETERS

Flood Susceptibility Parameters	**Low**	**Moderate**	**High**	**Very High**
A. Flood height	Areas likely to experience flood heights of less than 0.5 meter	Areas likely to experience flood heights of 0.5 to 1 meter	Areas likely to experience flood heights 1 to 2 meters	Areas likely to experience flood heights greater than 2 meters
B. Flood duration	Areas likely to experience flooding of less than 1 day	Areas likely to experience flooding of 1 to 3 days	Areas likely to experience flooding of more than 3 days	Areas likely to experience flooding of more than 3 days
C. Landform / Geomorphic feature	Low hills and gentle slopes	Fluvial terraces, alluvial fans and in-filled valleys	Topographic lows such as active and abandoned river channels, and areas along river banks	Topographic lows such as active and abandoned river channels, and areas along river banks
D. Drainage density	Sparse to moderately-spaced drainage	Moderately-spaced drainage	Closely-spaced drainage	Closely-spaced drainage
E. Prone to flashflood	No	No	No	Yes

Source: DENR – MGB Guidebook for the conduct of landslide and flood susceptibility assessment and mapping (1:10,000 scale)